10.1161/CIRCULATIONAHA.116.024754

Functional Definition of Progenitors Versus Mature Endothelial Cells Reveals Key SoxF-Dependent Differentiation Process

Running Title: *Patel et al.;Vascular Progenitors Define Endothelial Hierarchy*

Jatin Patel, PhD[1]; Elke J. Seppanen, PhD[1]; Mathieu P. Rodero, PhD[1]; Ho Yi Wong, BSc[1]; Prudence Donovan, PhD[2]; Zoltan Neufeld, PhD[3]; Nicholas M. Fisk, MBBS, PhD[1]; Mathias Francois, PhD[4]; Kiarash Khosrotehrani, MD, PhD[1,2]

[1]UQ Centre for Clinical Research, Experimental Dermatology Group, the University of Queensland, Brisbane, QLD, Australia;[2] UQ Diamantina Institute, Translational Research Institute, the University of Queensland, Woolloongabba, QLD, Australia;[3]School of Mathematics and Physics, the University of Queensland, Brisbane, QLD, Australia;[4]Institute of Molecular Biosciences, the University of Queensland, Brisbane, QLD, Australia

Address for Correspondence:
Kiarash Khosrotehrani, MD, PhD
UQ Centre for Clinical Research
Royal Brisbane and Women's Hospital
Building 71/918
Brisbane, Australia, 4029
Tel: +61-7-3346 6077
Fax: +61-7-3443 6966
Email: k.khosrotehrani@uq.edu.au

Journal Subject Terms: Angiogenesis; Cell Biology/Structural Biology; Endothelium/Vascular Type/Nitric Oxide; Stem Cells; Vascular Biology

Abstract

Background— During adult life, blood vessel formation is thought to occur via angiogenic processes involving branching from existing vessels. An alternate proposal suggests that neo-vessels form from endothelial progenitors able to assemble the intimal layers. We here aimed to define vessel-resident endothelial progenitors *in vivo* in a variety of tissues in physiological and pathological situations such as normal aorta, lungs, as well as wound healing, tumors and placenta.

Methods— Based on protein expression levels of common endothelial markers using flow cytometry, three sub-populations of endothelial cells could be identified among VE-Cadherin+ and CD45- cells.

Results— Lineage tracing using *Cdh5cre*^{ERt2}*/Rosa-YFP* reporter strategy demonstrated that the CD31-/loVEGFR2lo/intracellular endothelial population was indeed an endovascular progenitor (EVP) of an intermediate CD31intVEGFR2lo/intracellular transit amplifying (TA) and a definitive differentiated (D) CD31hiVEGFR2hi/extracellular population. EVP cells arose from vascular resident beds that could not be transferred by bone marrow transplantation. Furthermore, EVP displayed progenitor like status with a high proportion of cells in a quiescent cell cycle phase as assessed in wounds, tumors and aorta. Only EVP cells and not TA and D cells had self-renewal capacity as demonstrated by colony forming capacity in limiting dilution and by transplantation in Matrigel™ plugs in recipient mice. RNA sequencing revealed prominent gene expression differences between EVP and D cells. In particular, EVP cells highly expressed genes related to progenitor function including *Sox9*, *Il33, Egfr* and *Pdfgrα.* Conversely, D cells highly expressed genes related to differentiated endothelium including *Ets1&2*, *Gata2*, *Cd31, Vwf* and *Notch*. The RNA sequencing also pointed to an essential role of the *Sox18* transcription factor. SOX18's role in the differentiation process was validated using lineage-tracing experiments based on S*ox18Cre*^{ERt2}*/Rosa-YFP* mice. Besides, in the absence of functional SOX18/SOXF, EVP progenitors were still present, but TA and D populations were significantly reduced.

Conclusions—Our findings support an entirely novel endothelial hierarchy, from EVP to TA to D, as defined by self-renewal, differentiation and molecular profiling of an endothelial progenitor. This paradigm shift in our understanding of vascular resident endothelial progenitors in tissue regeneration opens new avenues for better understanding of cardiovascular biology.

Key Words: endothelial cell; angiogenesis; neovascularization; stem cell

Clinical Perspective

What is new?

- The discovery of an endovascular progenitor (EVP) cell *in vivo* that is present in normal endothelium (aorta, lung) and activated in vessel walls during various angiogenic situations (placenta, skin wound healing and tumors).
- The molecular definition of an endothelial hierarchy from an EVP to a mature differentiated endothelial cell via complete RNA-sequencing
- Clarification of the lineage of endothelial progenitors and their origin, using bone marrow transplantation and vascular specific lineage tracing mouse models to demonstrate that EVPs are derived neither from bone marrow nor from hematopoietic progenitors.

What are the clinical implications?

- Our study defines endothelial progenitors and is a major development into the understanding of how the vascular bed is able to remodel and/or regenerate during active angiogenesis in the adult.
- The discovery of an EVP will have significant implications for the development of endothelial progenitors as a cell therapy.

Introduction

The vascular system is an essential component of tissue homeostasis as well as the response to injury, given its widespread presence in most tissues. During embryonic development, vessels form from the periphery of blood islands as separate units that end up joining in a process called vasculogenesis [1]. However, in adults, formation of new blood vessels in response to insults or physiological signals is considered to result from the extension of existing vessels, defined as angiogenesis [2].

Neo-vessel formation has also been associated with activity of endothelial progenitors and their ability to assemble the intimal layers of mature vessels [1-4]. This initiated the concept that an endothelial progenitor with capacity to self-renew and form blood vessels, not only exists in adult tissues but can be transferred to a new environment to form neo-vessels, potentially recapitulating some features of vasculogenesis. However, the definition, cell lineage and possible hierarchy of such precursors remain controversial [3, 5, 6].

In particular, cells that promote angiogenesis, including myeloid cells and mesenchymal stem cells (MSC), have been often labeled as endothelial progenitors, despite their inability to form the endothelial layers of vessels *de-novo* [7, 8]. In fact, vascular endothelial cells and hematopoietic cells found in adult tissues often share common markers [5, 9]. Typically, positive surface expression of CD34, CD31 (PECAM1), VEGFR2 (flk1/KDR) and CD133 alone or in various combinations have been used to discriminate these progenitors [3, 10, 11], but are confounded by the presence of contaminating hematopoietic cells [5]. Therefore, a definitive marker to isolate endothelial progenitors is lacking and thus their lineage, whether hematopoietic or not, remains controversial [12]. It is therefore questionable whether a progenitor population with a unique potency to form new vessels exists *in vivo*.

To address the existence and definition of such endothelial progenitors *in vivo* in adults, we hypothesized that the existence of a progenitor within the endothelial compartment would result in a hierarchy among endothelial cells that would be reflected in heterogeneity of their cell surface markers. Given their presumed capacity, we also assumed such cells would be particularly active in situations of neo-vessel formation in adults. Based on this approach, we here define at the molecular level, a novel endovascular progenitor in mice which recapitulates some features of vasculogenesis and document both its self-renewal in transplantation experiments and its vascular capacity *in vivo* using lineage tracing.

Methods

Animals

All mice were treated in accordance with University of Queensland ethics approvals and guidelines for care of experimental animals. C57BL/6 mice (WT) (Animal Resources Centre, Perth, Western Australia), B6.Cg-Tg(Gt(ROSA)26Sor-EGFP)I1Able/J (ROSAeGFP) (The Jackson Laboratories, Bar Harbor, Maine, USA), and B6.SJL-Ptprc^{a}Pep3^{b}/BoyJArc (ptprc) (Animal Resources Centre, Perth, Western Australia) were used. For lineage tracing experiments *Sox18-Cre^{ERt2}* mice[13] and *Cdh5-cre^{ERt2}* were crossed with B6.Cg-*Gt(ROSA)26Sor$^{tm2(CAG-EYFP)Hze}$*/J (*ROSA$_{lox}$YFP$_{lox}$*) The resultant double transgenic offspring were named *Sox18-cre^{ERt2}/ROSA-YFP* (8-12 weeks old) and *Cdh5-cre^{ERt2}/ROSA-YFP*. For assessment of *Sox18* function, Ragged Opposum (*Sox18$^{Op/+}$*) mice and matched WT controls were used.

In vivo wound healing assay

Four full-thickness excisional wounds were generated down to the panniculus carnosus with a 6mm sterile punch biopsy (Stiefel Laboratories Inc., Research Triangle Park, NC, USA).

Wounds were left open and animals sacrificed at defined time-points post-wounding. To induce *Cre*-mediated recombination of YFP, 2mg tamoxifen (Sigma-Aldrich, St Louis, MO, USA) was injected intra-peritoneally. This was conducted for three consecutive days (D-3) prior to wounding or on the day of wounding (D0). Animals were sacrificed at D1, D3 and D5 post wounding.

In vivo tumor generation and Matrigel plugs

For generation of tumors, 5 x 10^5 B16F0 were injected subcutaneously into flanks of ROSAeGFP mice. Tumors were grown for 10 days before harvesting host-derived (GFP+) cell populations by flow sorting. Matrigel™ (Becton Dickinson, NJ, USA) plugs were generated by sub-cutaneous injection of Matrigel™ (4mg/ml) mixed with vehicle or individual flow sorted cell populations into each flank of WT mice. To assess maturity of neovessels formed, 75µg FITC-conjugated *Griffonia simplicifolia* isolectin B4 (Vector laboratories, CA, USA) was injected retro-orbitally 10mins before sacrificing animals with Matrigel™ plugs or in *Sox18* induced mice.

Bone marrow transplant

To generate BM chimeras ROSAeGFP were used as donors to ensure all transplanted cells were labeled uniformly with GFP[14]. In short, 5-week-old ptprc recipients were lethally irradiated with a total body dose of 1000 cGy as described in previous literature [15]. BM was harvested from the long bones of ROSAeGFP donors and a cell suspension containing 7 x 10^6 mononuclear cells administered via retro-orbital injection to irradiated recipients. After repopulation was confirmed, dorsal excisional wounds were generated on GFP+ BM chimeras.

Tissue processing of murine blood, bone marrow, placenta, aorta, wounds, tumors and Matrigel™ plugs from injured or uninjured animals.

Tissues were collected for *ex vivo* analyses at defined end points; wounds (D1-7), tumors (D10), Matrigel™ plugs (D3-14) and aorta (uninjured and D5). Total blood was collected via cardiac puncture, while one femur was flushed with a 27gauge needle and 5ml syringe to obtain total BM including endosteum. Excess skin surrounding individual wounds was removed and wounds were then minced through a 70μM cell strainer to generate single cell suspensions from wound granulation tissue. Red blood cells from total blood and BM preparations were lysed using a solution containing ammonium chloride, potassium bicarbonate and ethylenediaminetetraacetic acid (EDTA). Tumors and aorta were first digested for 1hr at 37°C in 1mg/ml collagenase I (Gibco, Life Technologies, NY, USA), 1mg/ml dispase (Gibco, Life Technologies, NY, USA), 150μg/ml DNase-I (Sigma-Aldrich, St Louis, MO, USA) before passing the suspension through a 70μM cell strainer. Lineage+ cells were then depleted from tumor cell suspensions via MACS® cell separation according to the manufacturer's instructions (Miltenyi Biotech, Cologne, Germany). Cell number and viability for each sample was assessed using 0.4% Trypan blue solution and a hemocytometer. Single cell suspensions were then used for flow sorting or analysis by flow cytometry.

Dissection of placentae from murine samples

Murine placentae were collected as previously described [16, 17]. Briefly, uterine horns were dissected from pregnant dams (E10.5-E18.5 days post-conception (d.p.c)) and concepti separated from the endometrium. Using fine forceps, the decidua was peeled away from individual concepti, exposing the embryo and placenta, contained within the yolk sac. The yolk sac was carefully removed and GFP+ placentae were selected using a long wave-length UV lamp. The

placentae were then carefully separated from the embryos, minced and incubated for 2hrs at 37°C with agitation as above before cell suspension prepared for analysis by flow cytometry

RNA Extraction

RNA was extracted from sorted EVP, TA and D cells using a QIAGEN mini kit (Qiagen, Valencia, CA) according to the manufacturer's instructions. RNA quality and concentration was assessed using the Agilent 2100 Bioanalyser (Agilent Technologies, Mulgrave, Victoria). 5-100ng of RNA was used for cDNA synthesis using the Superscript III Reverse Transcription Kit (Invitrogen, Mount Waverley, Australia).

Quantitative Polymerase Chain Reaction (qPCR)

Following cDNA synthesis, quantitative polymerase chain reaction (qPCR) assays were performed using SYBR® green chemistry according to manufacturers' instructions (Applied Biosystems, Foster City, CA, USA). The primer sequences are listed in Supplementary Table S3.

RNA sequencing

Total isolated RNA of appropriate RIN (>4) was prepared using the TruSeq stranded total RNA library prep kit as per manufacturer's instructions to be used in the Ilumina HiSeq2500 system by (Ilumina, San Diego, USA).

RNA sequencing analysis

Sequence data were aligned to GRCm38 with STAR (version 2.5.0c), and read counts were calculated using the GENCODE gene annotation (release M9). Differential expression was calculated with DESeq2 (version 1.6.2) [18, 19]. Significantly differentially expressed genes were selected by applied an FDR adjusted p-value cut off of $p<0.05$, and a log fold-change cut off of 2.

Flow Cytometry and FACS

Dissociated single cells in PBS/BSA/EDTA were incubated with various antibody combinations for multi-parameter flow acquisition and analysis.

A Gallios™ flow cytometer was used for sample acquisition while unbiased data analyses were performed with Kaluza® analysis software (Beckman-Coulter, Miami, Florida, USA). FACS was performed using a FACSaria cell sorter (Becton Dickinson, Franklin Lakes, NJ, USA). Extreme care was taken during cell sorting to ensure only 'singlets' were gated and any potential 'doublets' were gated out. Cell populations were collected in 5ml polypropylene tubes containing 100% fetal calf serum (FCS) or RNA lysis buffer for RNA extraction. Single cell confocal flow analysis was performed using ImageStream^{x} (Amnis Seattle, WA, USA). For each population, 30,000 single cells were analyzed.

The following combinations of antibodies were used to assess EPC populations:

EPC Combination: Rat anti-mouse VE-Cadherin FITC, VEGFR2 PE, CD31 PE-Cy7, CD34 Alexa647, and CD45 V450 (Becton Dickinson, NJ, USA).

EPC Characterisation: Rat anti-mouse CD11b PerCP, Tie2 PE, CD105 PE, CD73 PE, Sca1 PE, CD90.2 FITC, CD146 FITC (Becton Dickinson, NJ, USA).

EPC Cell cycle (Wounds, Aorta and Tumors): After first surface staining with the EPC panel, stained cells were fixed in 1% paraformaldehyde (PFA) and permeabilized in 1x Cytoperm buffer (Becton Dickinson, NJ, USA) before incubating in a solution containing 0.4mg/ml 4,6-diamidino-2-phenylindole, (DAPI) (Life technologies, CA, USA).

Immunohistochemistry

Dissected tissues were fixed for 2hrs in 4% PFA. The fixative was removed with 3x washes of PBS (Amresco, Solon, Ohio, USA). Tissues were subsequently infused with sucrose before cryo-

embedding. For specific antigen staining, cryo-sections were permeabilized in 0.5% Triton-x-100 (Chem Supply, Gillman, South Australia) before blocking with 20% normal goat serum. Paraffin-sections were deparaffinized and rehydrated. For this study, primary antibodies included rat anti-mouse CD31, rat anti-mouse VEGFR2, rat anti-mouse CD34, rat anti-mouse integrin α6 (CD49f) (all from Becton Dickinson); rabbit anti-mouse LYVE-1, rabbit anti-GFP (both from Abcam, MA, USA). Isotype control antibodies included rabbit and rat IgG. Excess and unbound antibody was then removed with 3x 5min washes in a solution containing 1x PBS/0.1% Tween-20 (Amresco, Solon, Ohio, USA). Secondary antibodies conjugated with Alexa-fluor 488 or 568 (Invitrogen, Carlsbad, CA, USA) were used for fluorescence detection. Briefly, sections were incubated with secondary antibodies for 40mins at room temperature. Excess antibody was removed by 3x washes in PBS/0.1% Tween-20. Nuclear staining was revealed in specimens mounted with ProLong® Gold mounting media containing DAPI (Invitrogen, Carlsbad, CA, USA). Confocal images were acquired with a Zeiss LSM 710 microscope equipped with Argon 561-10 nm DPSS and 633 nm HeNe lasers, and a 405-30 nm diode. We used the 405 nm diode laser for DAPI (detector 1, main beam filter MBS-405, 414–463-nm barrier filter), a 514-nm Argon line for YFP (detector 3, main beam filter MBS-458/514, 512-570-nm barrier filter) and the 561-nm photodiode laser for Alexa-568 (detector 3, main beam filter MBS-488/561, 562-611-nm barrier filter). Images or z-stacks (videos) were acquired using 20x or 40x objectives.

Whole mount wound preparation

Wound were excised on D5 as previously described before being fixed in 4% PFA for 2 h. Whole mount wounds approximately 5 mm thick were incubated at 4°C in FocusClear™ for 2 to 5 days (Celexplorer Labs Co, Taiwan). Samples were then mounted in the same medium on single concave microscope slides (Sail Brand, China).

In vitro colony formation assay: mouse

Endothelial colony formation was assessed using 2D Matrigel™ assays[20]. EVP, TA and D were sorted from tumors and seeded in plates containing complete EGM2 (with 10%FCS) medium (Lonza Australia Pty Ltd, Victoria, Australia). Cells were maintained at 37°C within an IncuCyte system (Essen Biosciences Ltd, Hertfordshire, United Kingdom) and imaged frequently over 7 days.

Mathematical modelling

Cell numbers from each population were modelled as absolute counts that could vary by proliferation, differentiation and apoptosis parameters. We compared two models: one with (A->B->C) and another without an intermediate population (A->B or C). Differentiation rates were used as variables to find the model that best fitted our experimental observations. Formulas are detailed in supplementary methods.

Statistical analysis

Statistical analyses were performed using GraphPad Prism v5c software. Data were analyzed using the following tests: Mann Whitney (for non-normally distributed data), and t-tests and 1-way or 2-way ANOVA with Bonferroni correction for normally distributed data. For the analysis of more than two groups with non-normally distributed data a Kruskal-Wallis was used with Dunn's post-hoc correction. A p-value <0.05 was considered significant.

Results

Identification and characterization of distinct populations among endothelial cells during neo-vessel formation in adults

We examined situations of neo-vessel formation in adults to explore the heterogeneity of endothelial cells. In single cell suspensions from several tissue types (in particular skin wounds), we initially ascertained using multi-parameter flow cytometry for individual markers the threshold gating in combination for CD34, CD45, CD31, VEGFR2 and VE-Cadherin staining using a fluorescence minus one (FMO) approach (Figure 1A-B). From set thresholds we were able to exclude contaminating hematopoietic cells by gating out CD45+ cells and simultaneously track markers commonly associated with endothelial cells: VE-Cadherin, CD34, CD31 and VEGFR2. To ensure their endothelial nature, we used a Lineage cocktail antibody (CD3, CD11b, CD45, Gr-1 and Ter-119) to more robustly discriminate and eliminate hematopoietic and in particular myeloid cells. Among Lineage- cells, those expressing either VEGFR2 or CD31 were in fact CD34+ (>90%) (Supplementary Figure S1A-B). In addition, CD34+ cells not expressing CD45 were almost exclusively VE-Cadherin+, strongly suggesting their endothelial nature (Figure 1B). Among CD45-CD34+ cells, three distinct sub-populations could be defined by their cell surface expression levels of VEGFR2 and CD31 (Figure 1C). Based on FMO analyses of CD31 and VEGFR2 levels, these populations were either CD31loVEGFR2-/lo, CD31intVEGFR2-/lo or CD31hiVEGFR2hi (Figure 1C). For simplicity we label these populations as EVP (Figure 1C light blue), TA, (Figure 1C purple) and D (Figure 1C dark blue) respectively. Such populations could also be clearly distinguished based on their relative expression of CD34 and CD31 when only CD45- cells were gated, further underpinning the existence of three distinct populations. Both EVP and D cells were CD34hi, whereas TA cells were CD34lo, confirmed by measuring Mean-Fluorescence-Intensity (MFI) across multiple experiments (Supplementary Figure S1C). Further characterization confirmed that all three populations homogenously expressed other endothelial markers such as Tie2 at the cell surface

(Supplementary Figure S1D; Table 1). Importantly, EVP cells did not express either mesenchymal (CD73) or pericyte (CD146) markers. In parallel, we also analyzed each population through flow-cytometry combined with quantitative image analysis (Amnis ®), which additionally validated the marker expression of each population (Supplementary Figure S1E). This also confirmed that all three populations had similar cell size and morphology in suspension. These cells differed from previously described populations of endothelial progenitors or mesoangioblasts, as they did not express c-kit and were unable to proliferate in mesenchymal-promoting media (data not shown)[21, 22].

Following from the observations of our endothelial populations in injury/vessel formation situations, we obtained aorta from uninjured mice to analyze for these endothelial populations. Here, we showed by gating on all VECAD+CD45- cells from the aorta the same endothelial populations (EVP, TA and D) plotted as either CD34/CD31 or CD31/VEGFR2 (Supplementary Figure S1F). This further suggests that the populations are vessel resident and may play a role in vessel maintenance during homeostasis. Finally, we assessed the existence of all three endothelial populations over a range of additional murine situations of vessel remodeling and active neo-vessel formation such as placenta, and tumor development as well as basally in uninjured murine aorta and lungs (Figure 1D). On each occasion all three endothelial populations were observed with only slight variation in levels of each marker as expected due to different tissue processing techniques.

Intracellular expression of CD31 and VEGFR2

We next evaluated whether the changes in CD31 or VEGFR2 levels reflected different cellular distribution of these surface markers and therefore assayed these populations for intracellular staining. The intracellular expression of CD31 remained consistent with membranous staining

confirming distinct populations based on discrete quantities of CD31 protein (CD31-/lo, CD31int and CD31hi) (Supplementary Figure S2A). However, VEGFR2 showed differential intracellular and cell surface levels. All three populations displayed VEGFR2 staining upon permeabilization although levels of CD31 did not differ. Image analysis (Amnis®) confirmed the vesicular distribution of intracellular VEGFR2 in each population (Supplementary Figure S2B). Furthermore, we quantified the intracellular versus membranous staining via image analysis using Amnis® to demonstrate clearly the observed difference in VEGFR2 expression between the two compartments, confirming the almost exclusive intracellular expression of VEGFR2 in EVP and TA populations (Supplementary Figure S2C; n=3). Overall, these results highlight differences between three populations of endothelial cells defined by their common expression of VE-Cadherin and absence of hematopoietic contamination. These three populations differ based on the level of CD34, CD31 as well as the cellular distribution and level of expression of VEGFR2 (n=3).

Kinetics of endothelial populations in wound angiogenesis

To decipher the contribution of these different endothelial populations to neo-vessel formation in adults, we explored their respective dynamics over time. Skin excisional wounds invariably form granulation tissue rich in CD31+VEGFR2+ vessels by day 5 (D5) post wounding, rendering this an attractive model to study the behavior of putative endothelial progenitors [23, 24] (Supplementary Figure S3A-C). In particular, the center of the granulation tissue remains devoid of any blood vessel up to D3-4 suggesting clearly that other vascularization processes than sprouting from vessels in the periphery of the wound can be studied in that area (Supplementary Figure S3C). The kinetics of endothelial populations in this setting proved dynamic and highly-reproducible (n>50) (Figure 2A). In gated CD45-CD34+ cells, the EVP population could be identified and

were predominant on D1-D2. TA but not D cells appeared more clearly from D2 in accordance with immunostaining on sections (Supplementary Figures S3A-B). From D3, all three populations were present. Expression levels of VEGFR2 and CD31 quantified by MFI were stable in each subpopulation over time, with the EVP population consistently negative and low for each marker respectively (Figure 2B). We examined the kinetics of all populations in the wound, both as absolute numbers and as proportion of CD34+CD45- cells (Figure 2C). Remarkably, the number of EVP cells remained low and did not vary from D2-5 (1-way ANOVA). TA and D cells increased in number, peaking on D5, in accordance with the expected peak of vascularization ($p=0.03$ and $p=0.001$ respectively compare to D1). Proportionally however, TA cells remained constant over time (1 way ANOVA) while D cells accumulated ($p<0.001$). This suggested that TA cells were an intermediate transit-amplifying population and that D cells were mature endothelial cells. This was supported by mathematical modelling where the best fit using the minimum mean square deviation method could be obtained for 24% of EVP cells differentiated into TA and 26% of TA cells differentiated into D at each increment of time (Supplementary Figures S4A-G; Supplementary Text; Supplementary Tables 1 & 2). In accordance, cell cycle analysis revealed that TA cells were more frequently in the S/G2/M phase in wounds but also in tumors and aorta (Figure 2D). Overall, the chronology of appearance, cell surface marker sequence, kinetics and mathematical modelling suggested a hierarchy and a differentiation sequence from EVP to D populations.

Origin of endothelial populations

Having established the heterogeneity of endothelial cells based on specific endothelial cell markers, we next investigated the origin of EVP cells that first appear in the healing wound. It has been proposed that endothelial progenitors transit in the circulation potentially contributing

to the pool of EVP cells at the beginning of the healing process. We first demonstrated that EVPs were of endothelial origin using a VE-Cadherin reporter (*Cdh5-cre^{ERt2}/ROSA-YFP)* mouse. Prior to wounding (D0), tamoxifen was administered for three consecutive days (Days -3 to -1), thus labelling >80% of VE-Cadherin+ cells with YFP. Flow cytometry analysis of the granulation tissue of wounds harvested at D1, D3 and D5, showed that most EVP cells were labelled with YFP at every single time point suggesting that they derived from VE-cadherin expressing endothelial cells (Figure 3A; n=5). To address definitively the tissue source of EVP cells participating in wound healing, we employed a bone marrow (BM) transplantation model where recipients were reconstituted with GFP+ BM cells (Figure 3B). Although such experiments have been performed previously [25], the results were never analyzed using multi-marker flow cytometry to exclude confounding BM-derived myeloid cells that co-express endothelial markers. Repopulation success (over 93% GFP chimerism in the BM) was validated 8 and 13 weeks post transplantation. Dorsal excisional wounds were then generated on chimeric recipients. All CD45-CD34+ cells present in wounds were GFP negative including the EVP, TA and D populations at both D1 and D5 post wounding, and 8 and 13 weeks after transplantation (Figure 3C). This indicated that BM does not contribute to endothelial cell populations and that these populations were neither contaminated by hematopoietic cells nor derived from them. As expected, CD45+ cells in wound granulation tissue were in part GFP+ (Figure 3C)[26]. Similarly, on sections, all blood vessels (in red) present in the granulation tissue (Figure 3D) or uninvolved skin (not shown) at D5 were negative for GFP. Of 116 CD31+ vessels recorded in the granulation tissue, no GFP+ vessel was identified. Confocal microscopy at single cell level revealed potential co-localization events instead to be circulating GFP+ cells only. These data

confirm that cells that form new vessels during wound angiogenesis are endothelial-derived and unlikely to be transferred by bone marrow transplantation.

Self-renewal capacity of endothelial populations

We next explored whether the above defined populations differed functionally. To perform transplantation and *in vitro* culture experiments, we isolated EVP, TA and D populations from normal aorta and from tumors induced in CAG-GFP transgenic mice ubiquitously expressing GFP (Figure 4A). In limiting dilution *in vitro* culture experiments, flow-sorted GFP+ tumor-derived or aorta-derived TA and D cells adhered and survived on Matrigel™ coated plates, but never proliferated. In contrast, isolated EVP cells clearly formed growing colonies over time and displayed tubes on their periphery. Quantification of the number of colonies per 1000 plated cells in limiting dilution assay robustly demonstrated that colony formation is a unique feature of the EVP cells only (Figures 4B-C). We estimated that the clonogenic capacity of an EVP to be 0.2-0.3% of cells plated, which was consistent between both tumor and aorta.

We next assessed the capacity of EVP, TA and D cells to self-renew and persist *in vivo*. Strikingly, despite transplanting similar numbers of each population in Matrigel™ plugs that were further implanted in nude mice *in vivo*, markedly-reduced numbers of GFP+ TA or D cells were retrieved after 7 days, compared to the EVP population ($n=5$, $p<0.01$) (Figures 4D-E). Indeed when EVP cells were transplanted, they formed in a Matrigel™ assay mostly EVP cells and some TA cells with fewer D cells as expected (not shown). Sections of the Matrigel™ plug showed that injected EVP cells identified by their GFP label could form CD31+ or VE-Cadherin+ vessels (Figure 4F). These data show that EVP cells are the only endothelial population with significant self-renewal potential and were therefore considered a potential endovascular progenitor.

Lineage tracing reveals endovascular progenitor mobilization in wound healing

Although the chronology of appearance and self-renewal hierarchy suggested that EVP cells gave rise to the other 2 populations, this remained to be formally demonstrated. We therefore conducted lineage tracing experiments using the VE-Cadherin reporter (*Cdh5-cre^{ERt2}/ROSA-YFP)* mouse and only administered tamoxifen at the time of wounding (D0). This was used to limit the labelling to only the few EVP cells present in the center of wounds at this very early time-point. As flow cytometry analysis demonstrated, >95% of all endothelial cells CD34+CD45-YFP+ were EVP cells at D1 (Figure 5A; n=5). This was confirmed by immunofluorescence of D1 wounds showing individual CD34+ YFP cells in the center of the granulation tissue that did not stain for CD45, CD31 or VEGFR2 (Figure 5B; n=3). At D5, entire YFP+ vessels labelled with both VEGFR2 or CD31 were then observed in the center of the granulation tissue co-stained with CD31 (Figure 5C&D; n=3). This strongly suggests that TA and D cells associated with these blood vessels and further detected in flow cytometry (Figure 5A), derived from the observed EVP cells in the center of the granulation tissue. Importantly no staining could be observed in the absence of tamoxifen injection or in mice lacking the Cre recombinase. These data confirm that vascular resident EVP mobilize during injury in the center of the granulation tissue to initiate neo-vessel formation within a wound healing setting. This occurs through a differentiation process towards a transitional population that is actively cycling (TA) and ends with a terminally differentiated population (D) based on kinetics.

Major gene expression differences between endovascular progenitors versus terminally differentiated endothelial cells from aorta

To assess the molecular differences between EVP and D populations (n=2; each n-equates to cell populations pooled from 30 mice) we isolated these individual populations from the aortas of

uninjured WT mice. Total RNA was extracted, depleted of ribosomal RNA and finally sequenced and analyzed demonstrating comparable clustering within each population (Figure 6A). Only genes that were >2 fold differentially expressed and with $p<0.05$ after multiple testing correction were gathered. This identified 860 genes identified as upregulated in D cells and 862 genes upregulated in EVP cells.

Directly from the sequencing analysis, *Pecam* (CD31) and *Kdr* (VEGFR2) as expected were strongly upregulated in the D as opposed to the EVP population (>35 fold). Also *Ptprc*, the gene encoding for the common leucocyte antigen CD45 was not expressed in significant levels in any of the populations reflecting the absence of hematopoietic contamination. In fact, many genes in the D population related to endothelial differentiation. These included key endothelial transcription factors such as *Ets1*, *Ets2*, *Gata2* and *Fli1* and importantly identifiable endothelial cell surface and functional markers such as *Cd31*, *Esam*, *Vwf*, *Tie1*, *Cldn5*, and *Enos*. Using qPCR to validate genes of interest, all were upregulated >5 fold compared to the EVP population (***$p<0.0001$) (Figure 6B). D cells were also found to over-express Notch signaling target genes (*Dll1*, *Dll4*, *Hes1*, *Hey1*), with all genes >5 fold upregulated compared to EVP (***$p<0.0001$; n=3). Lastly, the *soxF* family of genes including *Sox7*, *Sox17* and *Sox18* were observed as highly upregulated within the D population directly from RNA sequencing analysis. In fact, *Sox18* was shown to be >200 fold higher. Each *soxF* gene was subsequently validated through qPCR, with all genes being >10 fold higher within the D endothelial population (***$p<0.0001$; n=3).

In stark contrast, EVP cells did not express many adhesion molecules, but instead had over-representation of matrix metalloproteases (MMP) and growth factor signaling important in cell motion. MMP genes upregulated (>2.5fold) within the EVP population included *Mmp2*, *Mmp3*, *Mmp14*, *Mmp19* and *Mmp23*. Among notable genes, growth factor pathways such as

Egfr, *Pdgfrα* and *Pdgfrβ* were upregulated by 4, 20 and 6.5 fold respectively (Figure 6C), when compared with the D population (**p<0.01; n=3). Further to this, *Il33*, a known cytokine important in maintaining endothelial quiescence was also upregulated within the EVP population by 2 fold (**p<0.01; n=3), as was the transcription factor and known stem cell marker *Sox9* [27]. Using immunocytochemistry (n=3) to validate further some of the key genes identified, we demonstrated that IL33+ and SOX9+ staining was only observed on EVP cells (Figure 6D) and not on any D cells isolated through flow-sorting of normal aorta. However, when we stained for endothelial marker CD31, only D cells were positive (Figure 6D). This further validates our flow cytometry analysis demonstrating lack of CD31 cell surface expression among the EVP population. Nonetheless, EVP cells stained positively for VE-Cadherin as did D cells, demonstrating their isolation directly from a vascular source (Figure 6D).

Endovascular progenitors express Sox18 during wound revascularization

To further validate the gene expression differences obtained from RNA sequencing, we used another model to fate map the movement of EVP during a wound healing situation. The transcription factor SOX18 belongs to the SOXF group and is expressed in endothelial cell progenitors that instruct arterio-venous specification [28-30] and lymphatic endothelial cell fate during development [31]. The expression of SOX18 is not found at adult stage and is only re-activated in the endothelium under pathological conditions such as wound healing and tumor formation (Figure S5A)[31-35]. Given the strong differential expression of this gene between the D and EVP in normal aorta, we assumed that in a situation of active vessel formation, s*ox18* would be re-activated in those EVP cells entering transition towards a D differentiated fate.

In *Sox18-cre^{ERt2}/Rosa-YFP* reporter mice induced on a daily basis upon wound healing, YFP could only be visualized after tamoxifen induction (Supplementary Figure S5A) and was

restricted to CD31+ or VEGFR2+ expressing blood vessels at D3 and beyond (Supplementary Figure S5B). In particular, no expression could be observed in hair follicles if tamoxifen induction was performed after 3 weeks of age[36]. To address the timing of *Sox18* re-expression upon wounding and the hierarchy of endothelial cell populations, tamoxifen was administered in subsequent experiments to reporter mice at the time of wounding (D0) to induce *Cre*-mediated recombination only in cells present at this time-point (Figure 7A). Analysis on D1 after wounding and tamoxifen injection revealed the presence of YFP+ cells within the CD45-CD34+ population. All these cells were VE-Cadherin+. YFP+ cells could not be found in CD45-CD34- populations or in the absence of Cre recombinase (Figure 7B). Expression pattern of VEGFR2 and CD31 revealed that almost all YFP+ cells were from the EVP population at D1, with low CD31 and no surface VEGFR2 expression (Figure 7C). This confirmed that at least 30% of EVP cells at the beginning of the healing process, expressed *Sox18*. By D5, these YFP+ cells were still exclusively VE-Cadherin+ and all three populations, EVP, TA and D, could be observed suggesting the transition of EVP cells that re-activated *Sox18* expression to TA and D cells. Although wound vasculature is also derived from existing vessels, these form only from the periphery towards the center and are unlikely to contribute at early time points to vessels within the center of the granulation tissue (Supplemental Figure 3). Quantitatively, YFP labelled EVP cells reduced over time, whereas D cells increased markedly in proportion in agreement with the wound kinetics in Figure 5.

These findings were also consistent with observations on tissue sections after immunostaining for endothelial cell markers. On D1 within the granulation tissue, sparse single YFP+ cells were large elongated cells with sizeable dendrites staining exclusively for CD34 but not CD31 VEGFR2 nor CD45, corresponding as expected to the re-expression of *Sox18* in EVP

cells (Figure 7D). On D3 and D5, when looking at the center of the granulation tissue, these cells had formed vascular structures that expressed CD31 and VEGFR2 as TA and D cells (Figure 7D-E). This validated our initial lineage tracing using *Cdh5-cre^{ERt2}/ROSA-YFP* confirming that EVPs give rise to TA and D cells during neo-vessel formation. This further supported that YFP+ cells by flow cytometry (Figure 7B) and YFP+ vessels by D5 on sections (Figure 7F) represented similar proportions of the entire endothelial or vessel pool (about one third). Of note, YFP+ cells did not give rise to lymphatic vessels (LYVE1+) at D5.

We next injected isolectin B4 intravenously to label endothelial cells connected with the murine circulation. Isolectin B4 administered during wound healing on D3 labelled D cells and in part TA cells but not EVP cells by flow cytometry (Figure 7G). Similarly, isolectin B4 injection 3 days post wounding in *Sox18-cre^{ERt2}/Rosa-YFP* reporter mice induced at D0 with tamoxifen labelled only some YFP+ vessels reflecting different maturation status among YFP+ vessels derived from EVP cells (Figure 7H). This suggested a hierarchy of maturation as EVP containing vessels were not connected to the circulation and vessels containing D cells were mature and perfused.

SOXF family activity is essential for de novo vessel formation

Having established that *Sox18* expressing EVP cells could give rise to TA and D cells, we finally assessed SOX18 function in this differentiation process. We used the *Ragged Opposum* (*Sox18$^{Op/+}$*) mouse which harbors a dominant-negative mutation of SOX18. This model is the most severe situation of loss of SOX18/SOXF function, and obviates rescue mechanisms via SOX7 or SOX17 that often obscure the functional assessment of this family [37, 38]. Quantification of EVP, TA and D in *Sox18$^{Op/+}$* versus WT littermates revealed that although the number of EVP cells per wound was similar, there was a robust decrease in absolute numbers of TA and D cells

at D3 and D5 post-wounding ($p<0.001$), highlighting the reduced ability of the progenitors to generate D cells (Figure 8A). Furthermore, on D5, CD31+ and VE-Cadherin vessels were identified only at the periphery of *Sox18*$^{Op/+}$ wounds (Figure 8B) whereas granulation tissue of *Sox18*$^{Op/+}$ mice was devoid of any neo-vessel compared to WT littermates. This suggested that neo-vessels originating from EVP in the center of the granulation tissue depended almost exclusively on SOXF activity to generate the fully differentiated D cells that harbor high levels of SOXF.

Discussion

Repair and maintenance of the integrity of the vascular system after injury in adults has been deemed as relying solely on angiogenesis. This concept is challenged by the description of endothelial progenitors as an alternative source of neovessel formation. Others have pertained the concept of endothelial progenitors such as Ingram et al having previously observed the potential of endothelial precursors in human circulating blood and Naito et al describing the observation of an endothelial side population from numerous organ beds in mouse tissue[6, 20]. However, the lack of definition of such cells has left many questions unanswered, challenging the validity of this newer paradigm, especially in mice. Here we show that upon injury, adult endothelial cells are heterogeneous and can be grouped into three populations based both on their lack of hematopoietic markers and on their expression levels of CD34, CD31 and VEGFR2. In the temporally-defined context of wound healing, these three populations appeared sequentially in quantities suggestive of a hierarchy, as confirmed by lineage tracing using the *Cdh5-Cre*^{ERt2}*/ ROSA-YFP*. Furthermore, significant differences were observed in the gene expression make-up of EVP versus terminally-differentiated D cells. These differences readily defined each

population and further supported the 'progenitor' nature of an EVP cell. *Sox18* re-expression was shown to be an initial event present in progenitors with significant functional importance. Importantly, individual progenitors found in the center of wounds could be followed at later time points towards immature and then mature vessels connected to the circulation. Finally, colony forming capacity *in vitro* and engraftment and self-renewal *in vivo* were limited to this progenitor population.

Hierarchy not activation

An important issue has been the definition of endothelial progenitors. Indeed our observed maturation hierarchy could simply represent a sequence of activation [39]. Such hypothesis would however imply that any cell within the endothelial compartment would have an equal capacity to initiate an immature vessel as an EVP cell and go through the maturation hierarchy. We argue that the EVP cell population described here has inherent stem/progenitor cell characteristics. The evidence for this is that EVPs have a monopotent capacity to form definitive vessels even if injected as cells in suspension. Next, EVP cells have self-renewal capacity upon transfer in Matrigel™ plugs *in vivo*. In contrast, TA and D cells could not engraft in similar experiments nor could they produce EVP cells. Furthermore, EVP but not TA and D cells have *in vitro* colony forming capacity when isolated from either an active wound healing or basal aorta environment. This does not conflict with the relatively slow proliferation of EVP cells *in vivo*. Indeed, many described stem cell populations in the hematopoietic system or the skin are quiescent *in vivo* but have robust colony forming, proliferative and engraftment capacity [40, 41]. Although the *in vitro* clonogenic capacity of an EVP was approximately half compared to that of an endothelial side population as described by Naito et al[20], colonies were still obtained on each occasion of plating. Insofar, the *in vitro* methods used to determine colony-formation were entirely different, which

may attribute to the potential differences observed. The hierarchy described herein is thus not due to differential activation of these endothelial populations, but instead reflects an intrinsic cell characteristic that defines the EVP population as a stem/progenitor for the endothelial lineage.

Cellular origin of EVPs

We investigated whether bone marrow was the primary source of these endothelial progenitors during tissue repair using bone marrow chimeras. We took precautions in our bone marrow studies to use large gauge needles to include in the transfer the endosteal tissue where endothelium is expected to be found [42]. Similar to a previous study [25], we did not find donor derived blood vessels in wounds from bone marrow transplant recipients by confocal examination, and confirmed this using the more stringent criteria of flow cytometry. Using similar techniques, we reported previously donor-derived blood vessels in microchimeric situations, confirming our capacity to detect even rare events. In pregnant mice, fetal-derived endothelial CD34+CD45- progenitors formed entire blood vessels in wounds [43], inflamed skin [44] and tumors [45]. Although, undeniably a rare-event situation, we were nevertheless able to find the vessels emanating from these distant progenitors [43]. In the present study however, we could not find any donor-derived vessels, despite assessing a large number of sections, thus excluding any significant bone marrow or hematopoietic contribution to neo-vessel formation in this context.

Although the precise location of EVPs remains to be determined, we present evidence to suggest that these cells lie in existing vessels in the tissue surrounding the wound or the tumor. To address this question we used the vascular specific *Cdh5-Cre^{ERt2}/ ROSA-YFP*, a gold standard mouse model in tracing vascular populations [46]. This confirmed the migration of EVP cells into the center of the granulation tissue of D0 wounds. Furthermore, individual S*ox18*+ (YFP+) EVP cells could be identified at steady state or immediately upon wounding in uninjured vessels

surrounding the wound. It is highly likely that the EVP cells identified in the center of the wound derive from these isolated endovascular cells. Although wound vasculature is also derived from existing vessels, these act only from the periphery towards the center and are unlikely to contribute at early time points to vessels within the center of the granulation tissue. These data are in keeping with the increasing recognition of a population of vessel-resident endothelial progenitors [47, 48] and support the concept that local vessels, peripheral to the injury, could provide an immediate source of endothelial progenitors.

Distinct gene expression of EVP versus definitively differentiated D populations

RNA sequencing of sorted populations from normal aorta ascertained that the D population was a clearly differentiated endothelial population, demonstrating strong expression of key markers classically defining endothelial cells and their function. This included the transcription factor genes that control endothelial cell development and maturation [49, 50]. Collectively, there was also clear activation of the NOTCH pathway, which is indicative of the arterial phenotype but also instructive for the angiogenic pathway during tissue regeneration and endothelial cell proliferation [51, 52]. Most surprising was the identification of genes that delineated the EVP population. Many genes upregulated here were related to growth factor signaling, such as *pdgf* and *egf*. Both these pathways are potent activators in cell migration, stem cells populations, with roles in maintaining mesenchymal stem cell potency and self-renewal capacity, and in activating intestinal stem cells to mediate regenerative pathways [53, 54]. Furthermore, MMP genes were significantly upregulated in the EVP population. MMPs are known to initiate cell migration by allowing cells to degrade the surrounding extracellular matrix as well as enhancing cell engraftment during tissue regeneration. This has been demonstrated in models of cardiac regeneration with cardiac stem cells and *in vitro* using mesenchymal stem cells [55, 56]. We also

found here that EVP cells did not express hematopoietic markers and maintained low but significant levels of many endothelial markers usually absent in other mesenchymal populations such as CD31 or CD34.

Sox18-dependent control of TA and D identity

Our results confirm activation of *Sox18*, as previously reported in adult wounds and tumors. The importance of *sox18* transcription factor in the D population in normal endothelium as observed in the RNAseq analysis, was reflected in its expression in EVP cells potentially entering the differentiation process. Further studies are now indicated to identify the initial steps leading to selective activation of S*ox18* in a limited number of resident endothelial cells. Functionally, dominant negative mutation of SOX18 led to a significant depletion of both the TA and D populations. However, we were unable to discern the consequences of TA and D deficiency on wound closure in the model used due to the lack of hair follicle development in $Sox18^{op/+}$ mice. Although highlighting the functional importance of this transcription factor, the dominant negative nature of the mutation leaves open the possibility that SOX18 partners such as other SOXF family members may actually drive the observed function. Further studies need to address definitively the role of SOX18 binding partners in the transition from EVP to TA and D. Nevertheless, our study validates the functional importance of SOX18 and related partners in the hierarchy described here in endothelial cells.

In conclusion, we here define a novel population of vessel resident EVPs participating in pathological and physiological neovessel formation. Their molecular definition and sequential differentiation forming immature and then definitive vessels provides important insights in the activity of endothelial progenitors *in vivo*. This opens new avenues into the contribution of EVPs

to tissue repair, raising the potential for therapeutic modulation. Future studies will now look at the potency of EVP beyond its endothelial capacities.

Acknowledgements

We thank Paula Hall, from the QIMR Berghofer Medical Research Institute for technical assistance in flow sorting populations. We thank Dr. Lucie Leveque and Dr Kelli McDonald for providing access and assistance to an irradiator and the Amnis flow cytometry facility. We also thank the GUDMAP consortium for originally providing the *Sox18Cre^{ERt2}* mouse line.

Sources of Funding

This study was funded by a National Health and Medical Research Council of Australia (NHMRC) project grant (APP1023368), MF and KK salary was supported by NHMRC Career Development Fellowship (APP1011242 and APP1023371 respectively). JP salary was supported by the National Heart Foundation of Australia Postdoctoral Research Fellowship.

Disclosures

JP, KK and NMF are co-inventors on a patent licensed by AngioStem^{TM} relating to the isolation of endothelial progenitors from the placenta.

References

1. Flamme I, Frolich T and Risau W. Molecular mechanisms of vasculogenesis and embryonic angiogenesis. *J Cell Physiol*. 1997;173:206-210.
2. Carmeliet P. Angiogenesis in life, disease and medicine. *Nature*. 2005;438:932-936.
3. Asahara T, Murohara T, Sullivan A, Silver M, van der Zee R, Li T, Witzenbichler B, Schatteman G and Isner JM. Isolation of putative progenitor endothelial cells for angiogenesis. *Science*. 1997;275:964-967.
4. Krenning G, van Luyn MJ and Harmsen MC. Endothelial progenitor cell-based neovascularization: implications for therapy. *Trends Mol Med*. 2009;15:180-189.
5. Case J, Mead LE, Bessler WK, Prater D, White HA, Saadatzadeh MR, Bhavsar JR, Yoder MC, Haneline LS and Ingram DA. Human CD34+AC133+VEGFR-2+ cells are not endothelial progenitor cells but distinct, primitive hematopoietic progenitors. *Exp Hematol*. 2007;35:1109-1118.
6. Ingram DA, Mead LE, Tanaka H, Meade V, Fenoglio A, Mortell K, Pollok K, Ferkowicz MJ, Gilley D and Yoder MC. Identification of a novel hierarchy of endothelial progenitor cells using human peripheral and umbilical cord blood. *Blood*. 2004;104:2752-2760.
7. Wu Y, Chen L, Scott PG and Tredget EE. Mesenchymal stem cells enhance wound healing through differentiation and angiogenesis. *Stem Cells*. 2007;25:2648-2659.
8. Hirschi KK, Ingram DA and Yoder MC. Assessing identity, phenotype, and fate of endothelial progenitor cells. *Arterioscler Thromb Vasc Biol*. 2008;28:1584-1595.
9. Choi K, Kennedy M, Kazarov A, Papadimitriou JC and Keller G. A common precursor for hematopoietic and endothelial cells. *Development*. 1998;125:725-732.
10. Friedrich EB, Walenta K, Scharlau J, Nickenig G and Werner N. CD34-/CD133+/VEGFR-2+ endothelial progenitor cell subpopulation with potent vasoregenerative capacities. *Circ Res*. 2006;98:e20-25.
11. Peichev M, Naiyer AJ, Pereira D, Zhu Z, Lane WJ, Williams M, Oz MC, Hicklin DJ, Witte L, Moore MA and Rafii S. Expression of VEGFR-2 and AC133 by circulating human CD34(+) cells identifies a population of functional endothelial precursors. *Blood*. 2000;95:952-958.
12. Masuda H, Alev C, Akimaru H, Ito R, Shizuno T, Kobori M, Horii M, Ishihara T, Isobe K, Isozaki M, Itoh J, Itoh Y, Okada Y, McIntyre BA, Kato S and Asahara T. Methodological development of a clonogenic assay to determine endothelial progenitor cell potential. *Circ Res*. 2011;109:20-37.
13. Kartopawiro J, Bower NI, Karnezis T, Kazenwadel J, Betterman KL, Lesieur E, Koltowska K, Astin J, Crosier P, Vermeren S, Achen MG, Stacker SA, Smith KA, Harvey NL, Francois M and Hogan BM. Arap3 is dysregulated in a mouse model of hypotrichosis-lymphedema-telangiectasia and regulates lymphatic vascular development. *Hum Mol Gen*. 2014;23:1286-1297.
14. Giel-Moloney M, Krause DS, Chen G, Van Etten RA and Leiter AB. Ubiquitous and uniform in vivo fluorescence in ROSA26-EGFP BAC transgenic mice. *Genesis*. 2007;45:83-89.
15. Hill GR, Olver SD, Kuns RD, Varelias A, Raffelt NC, Don AL, Markey KA, Wilson YA, Smyth MJ, Iwakura Y, Tocker J, Clouston AD and Macdonald KP. Stem cell mobilization with G-CSF induces type 17 differentiation and promotes scleroderma. *Blood*. 2010;116:819-828.
16. Gekas C, Dieterlen-Lievre F, Orkin SH and Mikkola HK. The placenta is a niche for hematopoietic stem cells. *Dev Cell*. 2005;8:365-375.

17. Gekas C, Rhodes KE and Mikkola HK. Isolation and visualization of mouse placental hematopoietic stem cells. *Curr Protoc Stem Cell Biol*. 2008;Chapter 2:Unit 2A 8 1-2A 8 14.
18. Dobin A, Davis CA, Schlesinger F, Drenkow J, Zaleski C, Jha S, Batut P, Chaisson M and Gingeras TR. STAR: ultrafast universal RNA-seq aligner. *Bioinformatics*. 2013;29:15-21.
19. Love MI, Huber W and Anders S. Moderated estimation of fold change and dispersion for RNA-seq data with DESeq2. *Genome Biol*. 2014;15:550.
20. Naito H, Kidoya H, Sakimoto S, Wakabayashi T and Takakura N. Identification and characterization of a resident vascular stem/progenitor cell population in preexisting blood vessels. *EMBO J*. 2012;31:842-855.
21. Fang S, Wei J, Pentinmikko N, Leinonen H and Salven P. Generation of Functional Blood Vessels from a Single c-kit+ Adult Vascular Endothelial Stem Cell. *PLoS Biol*. 2012;10:e1001407.
22. De Angelis L, Berghella L, Coletta M, Lattanzi L, Zanchi M, Cusella-De Angelis MG, Ponzetto C and Cossu G. Skeletal myogenic progenitors originating from embryonic dorsal aorta coexpress endothelial and myogenic markers and contribute to postnatal muscle growth and regeneration. *J Cell Biol*. 1999;147:869-878.
23. Streit M, Velasco P, Riccardi L, Spencer L, Brown LF, Janes L, Lange-Asschenfeldt B, Yano K, Hawighorst T, Iruela-Arispe L and Detmar M. Thrombospondin-1 suppresses wound healing and granulation tissue formation in the skin of transgenic mice. *EMBO J*. 2000;19:3272-3282.
24. Zhang N, Fang Z, Contag PR, Purchio AF and West DB. Tracking angiogenesis induced by skin wounding and contact hypersensitivity using a Vegfr2-luciferase transgenic mouse. *Blood*. 2004;103:617-626.
25. Okuno Y, Nakamura-Ishizu A, Kishi K, Suda T and Kubota Y. Bone marrow-derived cells serve as proangiogenic macrophages but not endothelial cells in wound healing. *Blood*. 2011;117:5264-5272.
26. Rodero MP, Hodgson SS, Hollier B, Combadiere C and Khosrotehrani K. Reduced Il17a expression distinguishes a Ly6c(lo)MHCII(hi) macrophage population promoting wound healing. *J Invest Dermatol*. 2013;133:783-792.
27. Scott CE, Wynn SL, Sesay A, Cruz C, Cheung M, Gomez Gaviro MV, Booth S, Gao B, Cheah KS, Lovell-Badge R and Briscoe J. SOX9 induces and maintains neural stem cells. *Nat Neurosci*. 2010;13:1181-1189.
28. Pendeville H, Winandy M, Manfroid I, Nivelles O, Motte P, Pasque V, Peers B, Struman I, Martial JA and Voz ML. Zebrafish Sox7 and Sox18 function together to control arterial-venous identity. *Dev Biol*. 2008;317:405-416.
29. Cermenati S, Moleri S, Cimbro S, Corti P, Del Giacco L, Amodeo R, Dejana E, Koopman P, Cotelli F and Beltrame M. Sox18 and Sox7 play redundant roles in vascular development. *Blood*. 2008;111:2657-2666.
30. Sacilotto N, Monteiro R, Fritzsche M, Becker PW, Sanchez-Del-Campo L, Liu K, Pinheiro P, Ratnayaka I, Davies B, Goding CR, Patient R, Bou-Gharios G and De Val S. Analysis of Dll4 regulation reveals a combinatorial role for Sox and Notch in arterial development. *Proc Natl Acad Sci U S A*. 2013;110:11893-11898.
31. Francois M, Caprini A, Hosking B, Orsenigo F, Wilhelm D, Browne C, Paavonen K, Karnezis T, Shayan R, Downes M, Davidson T, Tutt D, Cheah KS, Stacker SA, Muscat GE, Achen MG, Dejana E and Koopman P. Sox18 induces development of the lymphatic vasculature in mice. *Nature*. 2008;456:643-647.

32. Darby IA, Bisucci T, Raghoenath S, Olsson J, Muscat GE and Koopman P. Sox18 is transiently expressed during angiogenesis in granulation tissue of skin wounds with an identical expression pattern to Flk-1 mRNA. *Lab Invest*. 2001;81:937-943.
33. Young N, Hahn CN, Poh A, Dong C, Wilhelm D, Olsson J, Muscat GE, Parsons P, Gamble JR and Koopman P. Effect of disrupted SOX18 transcription factor function on tumor growth, vascularization, and endothelial development. *J Natl Cancer Inst*. 2006;98:1060-1067.
34. Duong T, Proulx ST, Luciani P, Leroux JC, Detmar M, Koopman P and Francois M. Genetic ablation of SOX18 function suppresses tumor lymphangiogenesis and metastasis of melanoma in mice. *Cancer Res*. 2012;72:3105-3114.
35. Deng Y, Atri D, Eichmann A and Simons M. Endothelial ERK signaling controls lymphatic fate specification. *J Clin Invest*. 2013;123:1202-1215.
36. Legrand JM, Roy E, Ellis JJ, Francois M, Brooks AJ and Khosrotehrani K. STAT5 Activation in the Dermal Papilla Is Important for Hair Follicle Growth Phase Induction. *J Invest Dermatol*. 2016;136:1781-1791.
37. Hosking B, Francois M, Wilhelm D, Orsenigo F, Caprini A, Svingen T, Tutt D, Davidson T, Browne C, Dejana E and Koopman P. Sox7 and Sox17 are strain-specific modifiers of the lymphangiogenic defects caused by Sox18 dysfunction in mice. *Development*. 2009;136:2385-2391.
38. Pennisi D, Bowles J, Nagy A, Muscat G and Koopman P. Mice null for sox18 are viable and display a mild coat defect. *Mol Cell Biol*. 2000;20:9331-9336.
39. Hellstrom M, Phng LK and Gerhardt H. VEGF and Notch signaling: the yin and yang of angiogenic sprouting. *Cell Adh Migr*. 2007;1:133-136.
40. Foudi A, Hochedlinger K, Van Buren D, Schindler JW, Jaenisch R, Carey V and Hock H. Analysis of histone 2B-GFP retention reveals slowly cycling hematopoietic stem cells. *Nature Biotechnol*. 2009;27:84-90.
41. Tumbar T, Guasch G, Greco V, Blanpain C, Lowry WE, Rendl M and Fuchs E. Defining the epithelial stem cell niche in skin. *Science*. 2004;303:359-363.
42. Kopp HG, Avecilla ST, Hooper AT and Rafii S. The bone marrow vascular niche: home of HSC differentiation and mobilization. *Physiology*. 2005;20:349-356.
43. Nassar D, Droitcourt C, Mathieu-d'Argent E, Kim MJ, Khosrotehrani K and Aractingi S. Fetal progenitor cells naturally transferred through pregnancy participate in inflammation and angiogenesis during wound healing. *FASEB J*. 2012;26:149-157.
44. Nguyen Huu S, Oster M, Uzan S, Chareyre F, Aractingi S and Khosrotehrani K. Maternal neoangiogenesis during pregnancy partly derives from fetal endothelial progenitor cells. *Proc Natl Acad Sci U S A*. 2007;104:1871-1876.
45. Nguyen Huu S, Oster M, Avril MF, Boitier F, Mortier L, Richard MA, Kerob D, Maubec E, Souteyrand P, Moguelet P, Khosrotehrani K and Aractingi S. Fetal microchimeric cells participate in tumour angiogenesis in melanomas occurring during pregnancy. *Am J Pathol*. 2009;174:630-637.
46. Alva JA, Zovein AC, Monvoisin A, Murphy T, Salazar A, Harvey NL, Carmeliet P and Iruela-Arispe ML. VE-Cadherin-Cre-recombinase transgenic mouse: a tool for lineage analysis and gene deletion in endothelial cells. *Dev Dyn*. 2006;235:759-767.
47. Ingram DA, Mead LE, Moore DB, Woodard W, Fenoglio A and Yoder MC. Vessel wall-derived endothelial cells rapidly proliferate because they contain a complete hierarchy of endothelial progenitor cells. *Blood*. 2005;105:2783-2786.

48. Kovacic JC and Boehm M. Resident vascular progenitor cells: an emerging role for non-terminally differentiated vessel-resident cells in vascular biology. *Stem Cell Res*. 2009;2:2-15.
49. Kumar AH and Caplice NM. Clinical potential of adult vascular progenitor cells. *Arterioscler Thromb Vasc Biol*. 2010;30:1080-1087.
50. De Val S and Black BL. Transcriptional control of endothelial cell development. *Dev Cell*. 2009;16:180-195.
51. Hofmann JJ and Iruela-Arispe ML. Notch signaling in blood vessels: who is talking to whom about what? *Circ Res*. 2007;100:1556-1568.
52. Ramasamy SK, Kusumbe AP, Wang L and Adams RH. Endothelial Notch activity promotes angiogenesis and osteogenesis in bone. *Nature*. 2014;507:376-380.
53. Ball SG, Shuttleworth A and Kielty CM. Inhibition of platelet-derived growth factor receptor signaling regulates Oct4 and Nanog expression, cell shape, and mesenchymal stem cell potency. *Stem Cells*. 2012;30:548-560.
54. Gregorieff A, Liu Y, Inanlou MR, Khomchuk Y and Wrana JL. Yap-dependent reprogramming of Lgr5(+) stem cells drives intestinal regeneration and cancer. *Nature*. 2015;526:715-718.
55. Shen D, Tang J, Hensley MT, Li T, Caranasos TG, Zhang T, Zhang J and Cheng K. Effects of Matrix Metalloproteinases on the Performance of Platelet Fibrin Gel Spiked With Cardiac Stem Cells in Heart Repair. *Stem Cells Transl Med*. 2016;5:793-803.
56. Schultz KM, Kyburz KA and Anseth KS. Measuring dynamic cell-material interactions and remodeling during 3D human mesenchymal stem cell migration in hydrogels. *Proc Natl Acad Sci U S A*. 2015;112:E3757-3764.

Table 1. Cell surface marker expression

MARKER	EVP	TA	D
VECAD	+++	+++	+++
CD34	+++	+	+++
CD31	-/+	++	+++
VEGFR2	-	+	+++
CD45	-	-	-
Tie2	+++	+++	+++
Alpha-6	-	+	+++
CD73	-	-	++
CD105	-	+	+++
Sca1	+++	+++	+++
CD90.2	+++	+++	+++
CD146	-	+	+++

+ Positive Staining; - Negative Staining
EVP – Endovascular Progenitor;
TA – Transit Amplifying;
D – Definitive Differentiated

Figure Legends

Figure 1. Identification and characterization of distinct populations among endothelial cells in adults. A: Fluorescence-Minus-One (FMO) analyses were performed on cells from D5 wounds in order to set threshold for CD45 and CD34 positivity (dotted red line marks threshold). A clear population could be distinguished in the CD34+CD45- quadrant gated on live cells. B: All cells from the CD34+CD45- populations were shown to be vascular in origin as demonstrated by VE-Cadherin (VECAD) positivity. C: Fluorescence-Minus-One (FMO) analyses were performed on endothelial CD34+CD45- cells in order to set threshold for CD31 and VEGFR2 positivity. In gated CD34+CD45- cells, three distinct populations were observed based on CD31 and VEGFR2 expression in wounds (from left to right: EVP, TA and D; n>50). D: Gating on cells that are only CD34+CD45-VECAD+, the 3 endothelial populations can be demonstrated in four other angiogenic situations: aorta, lung, E18 placenta and tumors. EVP – Endovascular Progenitor; TA – Transit Amplifying; D – Definitive Differentiated

Figure 2. Kinetics of endothelial populations in wound angiogenesis. A: Gated on all CD34 +CD45- endothelial cells, days 1- 7 flow plots demonstrate the kinetics of EVP, TA and D cells in skin wounds (n=3 to >50 per time point). B: Quantification of Mean-Fluorescence-Intensity (MFI) values of CD31 and VEGFR2 further confirmed the stability of expression levels of these endothelial markers in the three populations over time through the wound kinetic study (n=6). Results presented as mean +/- SEM. C: Absolute numbers (left) (**p<0.01 vs EVP; n=6) and relative proportions (right) of EVP, TA and D in 6mm punch biopsy wounds over time (n=6). D: Cell cycle analysis using DAPI quantification of nucleic acids per cell demonstrated

that more EVP cells were in G0/1 phase (###p<0.001 vs. TA; ***p<0.001 vs D) whereas more TA cells in the S+ G2/M phase (###p<0.001 vs. EVP; ***p<0.001 vs D n=6) from both wounds and tumors. Results presented as mean +/- SEM. EVP – Endovascular Progenitor; TA – Transit Amplifying; D – Definitive Differentiated

Figure 3. Origin of the endothelial populations. A: Schematic representation of the lineage tracing model employing the *Cdh5-cre^{ERt2}/Rosa-YFP* mouse model. All animals were induced with tamoxifen daily during 3 days prior to wounding (D-3 to D0). At D0 mice were wounded. YFP expression was analyzed and compared between CD34-CD45-, CD34+CD45- and finally reported to CD34+CD45- in Cre negative control mice at day (D) 1, 3 and 5. Only D5 results are displayed as comparative histograms but results were concordant. YFP+ cells were only observed in CD34+CD45- with Cre induction demarcated by yellow on the histogram. There were no YFP+ cells in animals that did not have any Cre activity (white). YFP+CD34+CD45- form the proposed endothelial hierarchy as seen by EVP cells at D1 (n=3) and EVP, TA and D by D5 (n=3). **B:** Schematic representation to address the origin of EVP through the use of a GFP-bone marrow transplantation model. Mice were wounded at either 8 or 13 weeks post-transplantation of whole bone marrow including the endosteal layer (n=20).

C: Flow analysis of days (D) 1 and D5 wounds from transplanted mice: all CD34+CD45-within the wound granulation tissue were GFP negative and not bone marrow derived (n=20).

D: By immunofluorescence and confocal microscopy imaging, all CD31+ mature vessels within the wound at D5 were also GFP negative. High magnification images further highlighted the GFP- nature of the CD31+ vessels. Only individual GFP+CD31+ cells could be observed as

marked by dotted white arrows (Scale bar represents 150μm and 50μm respectively; n=6). YFP – Yellow fluorescent protein. EVP – Endovascular Progenitor

Figure 4. Self-renewal capacity of endothelial populations. A: Schematic diagram demonstrating the isolation of GFP+ EVP, TA, and D, from tumors (n>40). **B-C:** Limiting dilutions of endothelial cells from each population were cultured on Matrigel™ coated plates and followed over time to obtain distinct single colonies. Time-lapse (hours) imaging demonstrated only colony formation when GFP+ EVP cells were plated. A representative clone is figured **(B)** (n=3) and **(C)** quantitative colony forming capacity of EVP, TA and D from tumors and aorta in limiting dilution (##p<0.05 vs TA; *p<0.05 vs D) (Scale bar represents 70μm; n=3). **D-E:** Representative dot plots of cell suspensions obtained from Matrigel™ plugs implanted in mice and containing GFP+ EVP, TA and D cells (n=5) **(D)** and **(E)** percentage recovery of each population following transplantation as reported to the initial number of cells injected (n=5) (##p<0.01 vs TA; **p<0.01 vs D). **F:** CD31/VE-Cadherin (VECAD) staining of GFP+EVP population derived vessels in Matrigel™ (Scale bars represent 150μm and 50μm) (n=5). Top row of images demonstrate that not all CD31 vessels in the Matrigel™ plugs were GFP+. Bottom two rows are high magnification images of vessels from top row showing double staining of GFP/CD31 or GFP/VECAD. Results are presented as mean and distribution. EVP – Endovascular Progenitor; TA – Transit Amplifying; D – Definitive Differentiated; GFP – Green Fluorescent Protein. A568 – Alexa 568 dye in secondary stain (Red).

Figure 5. Lineage tracing reveals endovascular progenitor mobilization in wound healing.

A: Schematic representation of the lineage tracing model employing the *Cdh5-cre^{ERt2}/Rosa-YFP*

mouse model. All animals were induced with tamoxifen and wounded at day 0 (D0). Absence of YFP expression was verified on CD34-CD45- cells and in Cre negative control mice at day (D) 1 and 5. Only D5 results are displayed but results were concordant. YFP+ cells were only observed in CD34+CD45- with Cre induction demarcated by yellow on the histogram. There were no YFP+ cells in animals that did not have any Cre activity (white). YFP+CD34+CD45- were observed and related solely to EVP cells at D1, EVP and TA cells at D3 (n=3) and EVP, TA and D by D5 (n=3). **B-C:** Within the center of the granulation tissue (GT) of wounds, immunofluorescence demonstrated YFP+ cells at D1 are isolated CD34+, CD31/VEGFR2/CD45 negative cells (Scale bar represents 50μm; n=5). By D3 entire YFP+ vessels can be observed and are CD31 positive (Scale bar represents 50μm; n=5). **D:** Low magnification image of the center of the GT demonstration YFP+ vessels co-staining with CD31 (Scale bar represents 100μm). EVP – Endovascular Progenitor; TA – Transit Amplifying; D – Definitive Differentiated; YFP – Yellow fluorescent protein; A568 – Alexa 568 secondary stain (Red).

Figure 6. Major gene expression differences between endovascular progenitors versus terminally differentiated endothelial cells from aorta. A: Following RNAseq analysis, there was considerable gene expression clustering representative of each population; EVP and D (n=2). **B:** Validation of gene of interest from the D population was conducted: *Ets1*, *Ets2*, *Gata2*, *Fli1, Cd31*, *Esam*, *Vwf*, *Tie1*, *Cldn5*, *Enos, Dll1*, *Dll4*, *Hes1* and *Hey1* were all upregulated >5 fold (***p<0.001; n=3) and *Sox7*, *Sox17* and *Sox18* were upregulated >10 fold in comparison to EVP (***p<0.001; n=3). **C:** Validation of gene of interest from the EVP population was conducted: *Egfr, Pdgfrα, Pdgfrβ, Il33* and *Sox9* were all upregulated >2 fold in comparison to D (**p<0.01; n=3). **D:** Immunostaining was conducted on EVP and D cells isolated from aorta.

IL33 and SOX9 was only observed on EVP but not D cells, further validating the RNAseq data. EVP did not stain for CD31 but were positive for VE-Cadherin. D cells stained for both CD31 and VE-Cadherin (Scale bar represents 50μm; n=3). EVP – Endovascular Progenitor; TA – Transit Amplifying; D – Definitive Differentiated; A488 – Alexa 488 secondary stain (green); A568 – Alexa 568 secondary stain (Red).

Figure 7. Lineage tracing reveals the role of *sox18* in the endothelial maturation hierarchy.

A: Schematic representation of the lineage tracing model employing the *Sox18-cre^{ERt2}/Rosa-YFP* mouse model. All animals were induced with tamoxifen at day (D) 0 upon wounding.

B: YFP expression was analyzed on three populations CD34-CD45-, CD34+CD45- and reported to CD34+CD45- in Cre negative control mice at days (D) 1 and 5. Only D5 results are displayed but results were concordant. YFP+ cells were only observed in CD34+CD45- with Cre induction demarcated by yellow on the histogram. There were no YFP+ cells in animals that did not have any Cre activity (white). All YFP+CD34+CD45- cells were vascular in origin with 100% of these cells positive for VE-Cadherin (VECAD) expression. **C:** YFP+CD34+CD45- were observed and related solely to EVP cells at D1 (n=3) and EVP, TA and D by D5 (n=3). Relative proportions of each population was measured at D1 and D5, demonstrating a reduction in EVP and a subsequent increase in D over time. Results presented as mean +/- SD.

D: Within the center of the granulation tissue (GT) of wounds, immunofluorescence demonstrated YFP+ *Sox18* expressing cells at D1 are CD34+, CD31/VEGFR2/CD45 negative (Scale bar represents 50μm; n=5). By D3 entire vessels were observed as CD31 and VEGFR2 positive (Scale bar represents 50μm; n=5). **E:** At D5 YFP+ vessels were CD31+/VEGFR2+/VECAD+ but negative for lymphatic marker LYVE-1 (Scale bar 50μm;

n=5). **F:** Quantification of CD31+YFP+ (27.5%; Dotted white arrow) vessels in D5 granulation tissue (GT) of wounds via immunofluorescence (Dotted green arrow CD31+ only; Dotted white line demarcates edge of wound; Scale bar represents 150μm; n=5; Mean +/- SEM). **G,** Lineage tracing was performed as described and isolectin B4 was delivered 10 minutes prior to tissue collection on D3 post wounding. Histogram showing EVP as isolectin negative, and TA and D as isolectin positive; immunofluorescence showing isolectin negative (white arrows) YFP+ vessels in D3 wounds (Scale bar represents 50μm; n=2). Results presented as mean +/- SEM. EVP – Endovascular Progenitor; TA – Transit Amplifying; D – Definitive Differentiated; YFP – Yellow Fluorescent Protein; A568 – Alexa 568 secondary stain (Red).

Figure 8. SOXF family activity is essential for de novo vessel formation. A: To determine whether *Sox18* plays a role in maturation in the endothelial hierarchy we used the SOX18 dominant negative mutant mice ($Sox18^{Op+}$) and compared to wild type littermate controls. At days (D) 1, 3 and 5 wounds were harvested and absolute numbers of EVP, TA and D from wild-type (WT) and $Sox18^{op/+}$ mice were measured by flow cytometry. Numbers of EVP were comparable between WT and $Sox18^{op/+}$, however significant differences were observed in absolute numbers of TA and D, demonstrating a potential maturation dysfunction in the $Sox18^{op/+}$ (n=5) (***p<0.001). **B:** CD31 staining (red) in the center of granulation tissue (GT) from D5 wounds of WT mice displays large numbers of vessels, whereas an absence of both mature CD31 or VE-Cadherin (VECAD) (red) vessels in the center of the GT can be seen from $Sox18^{op/+}$ mice. Wound edges are demarcated by white dotted lines (Scale bar represents 150μm; n=3)**.** Results presented as mean +/- SEM. EVP – Endovascular Progenitor; TA – Transit Amplifying; D – Definitive Differentiated.

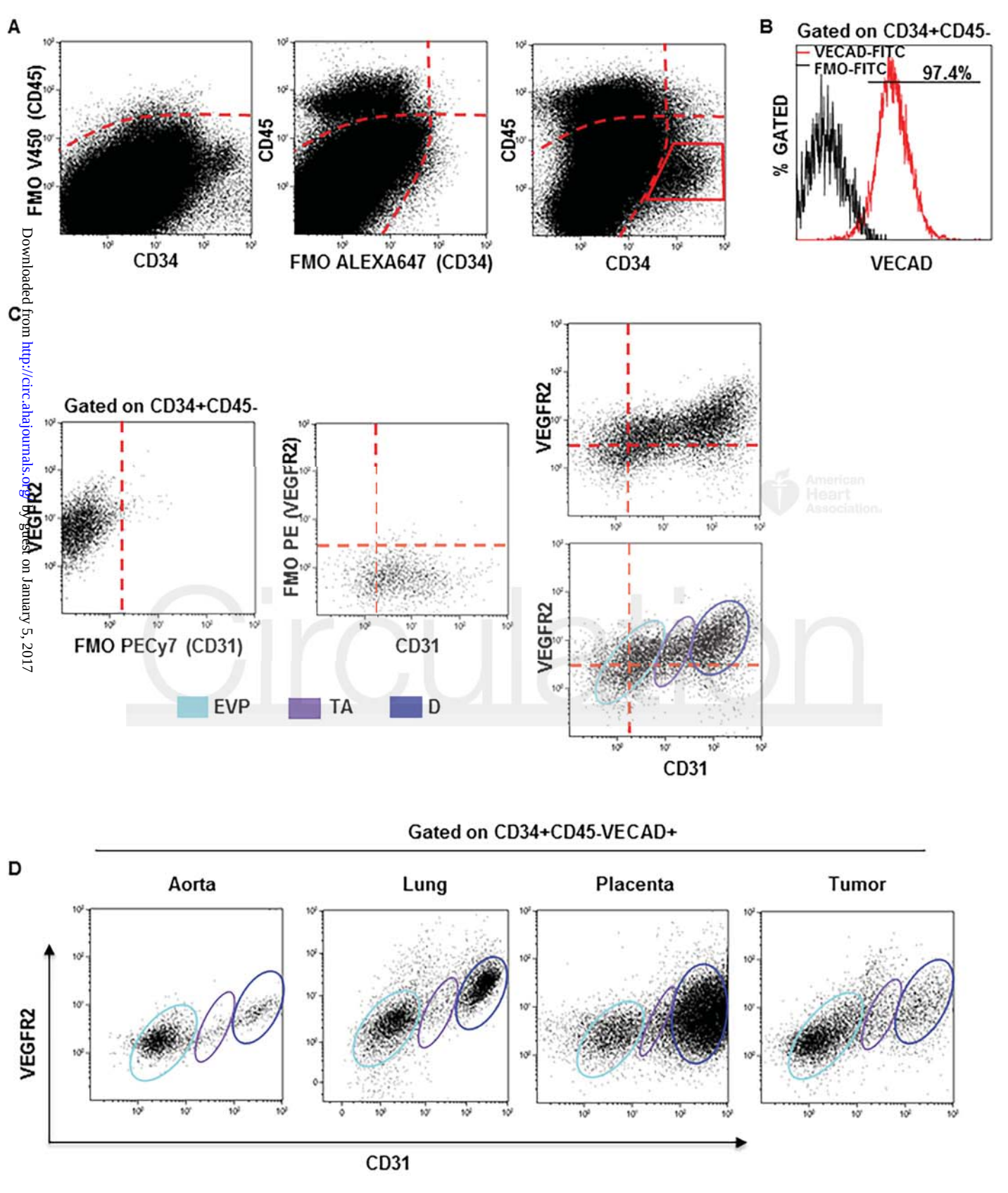

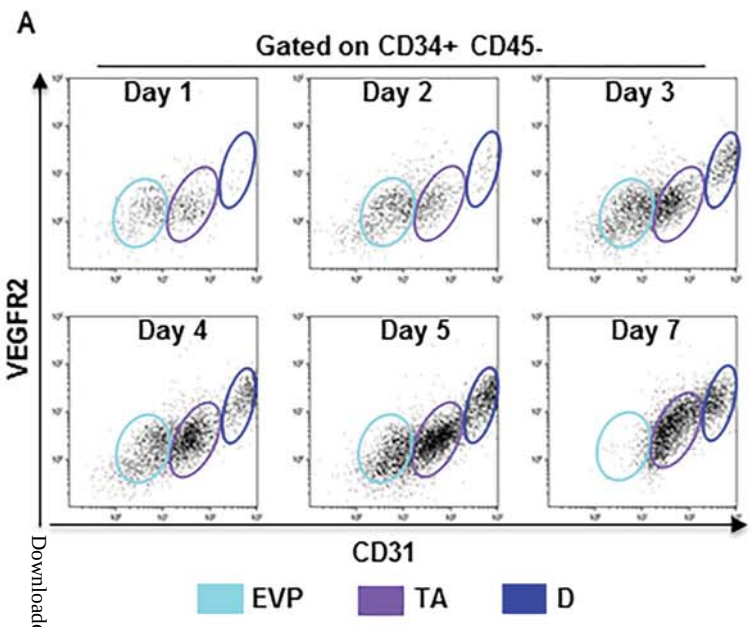

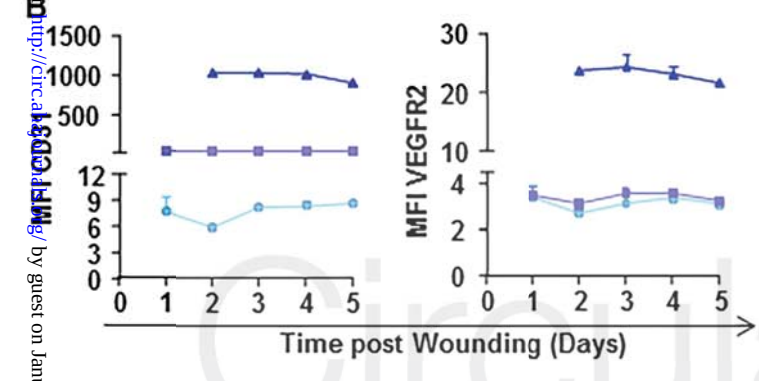

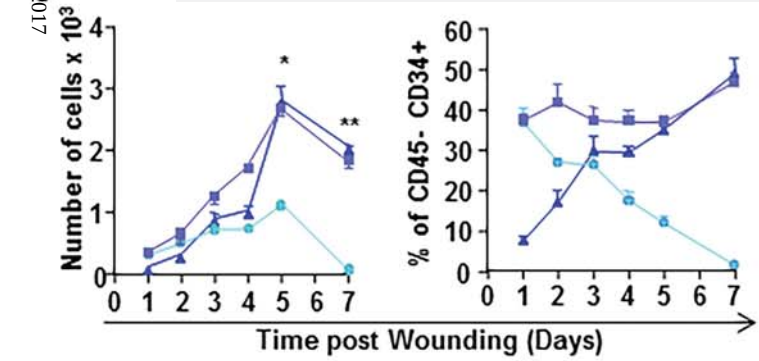

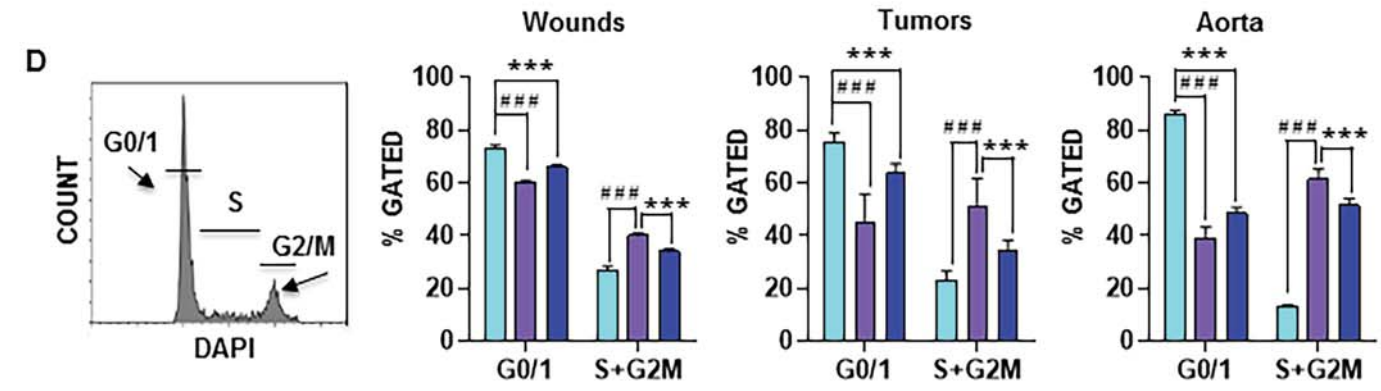

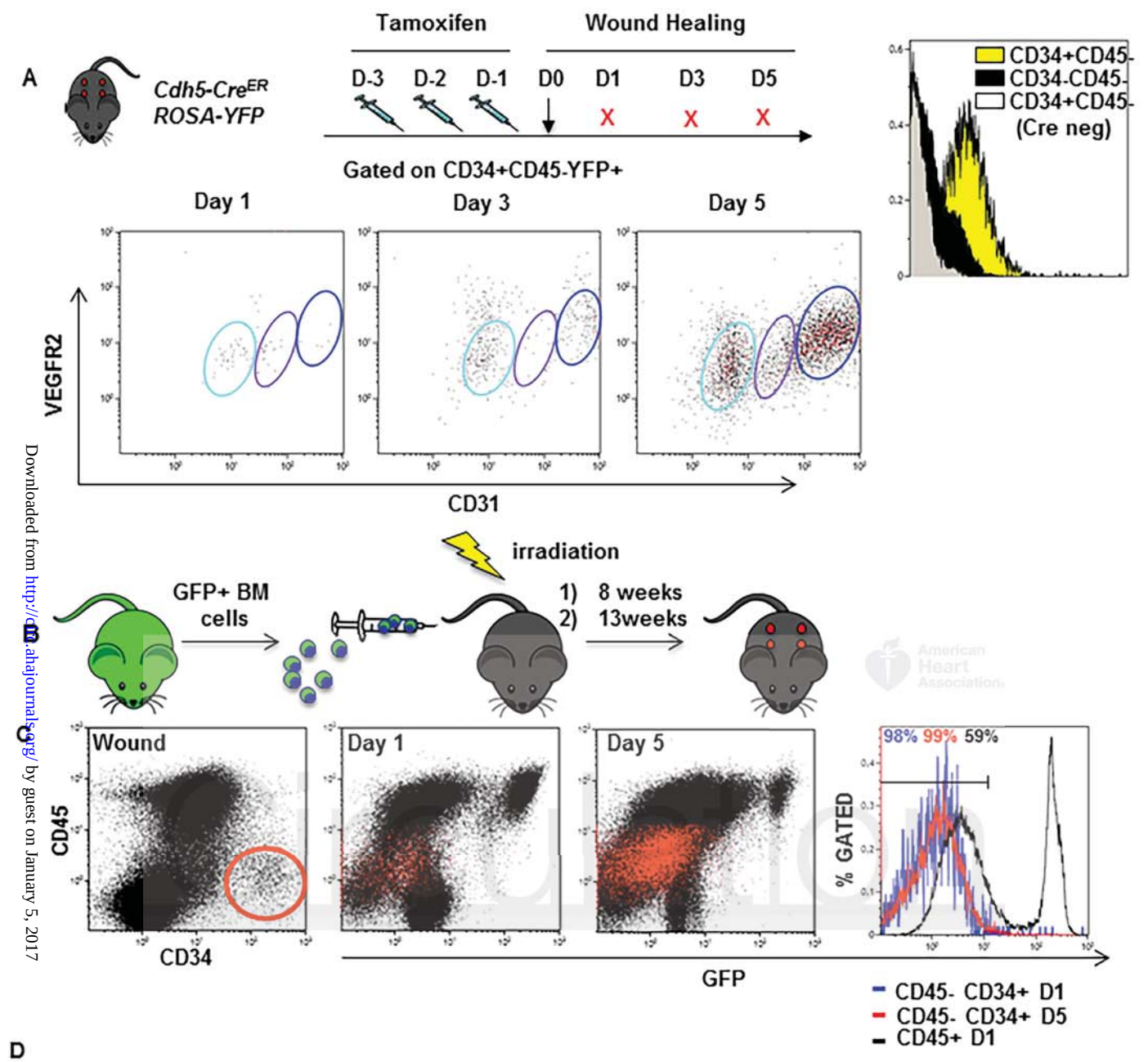

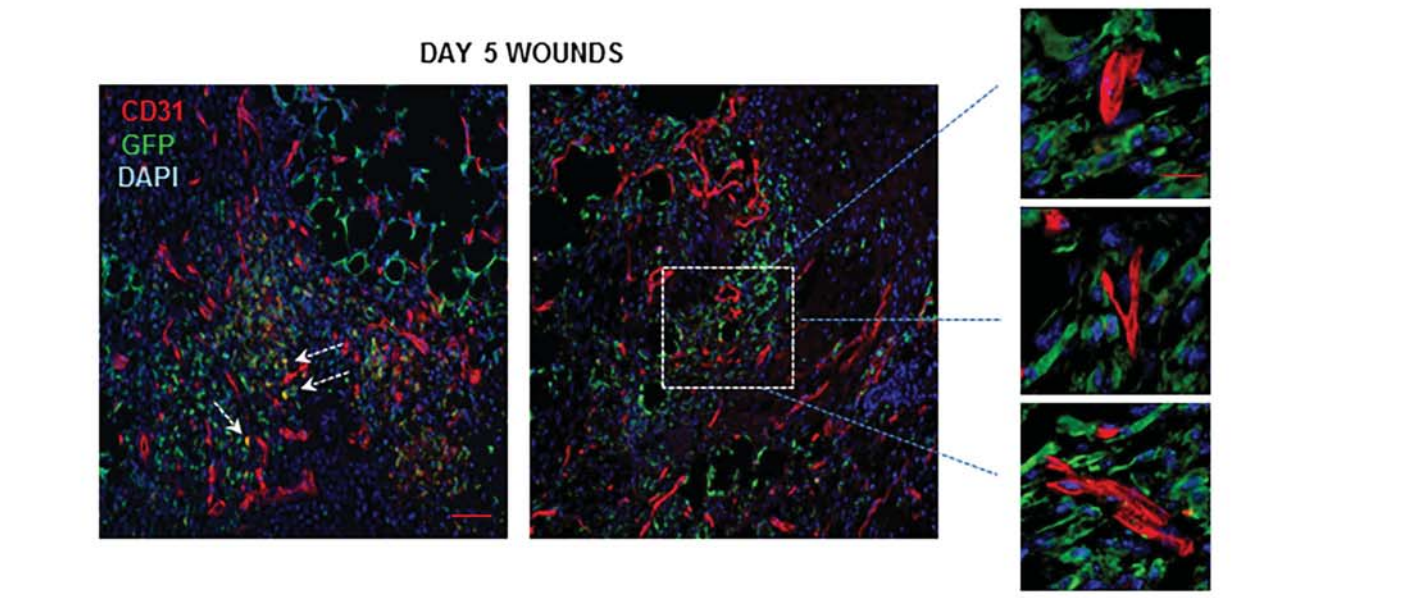

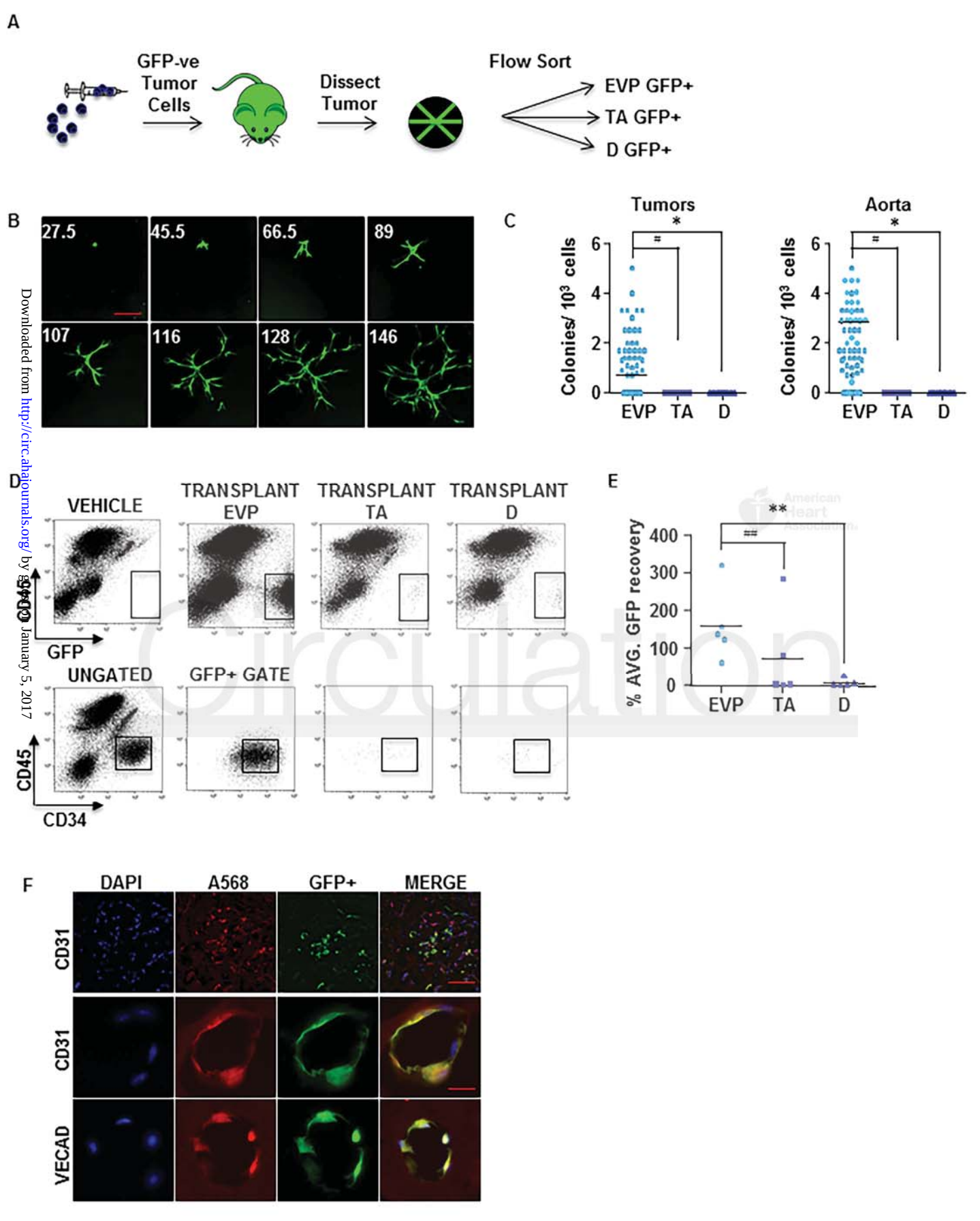

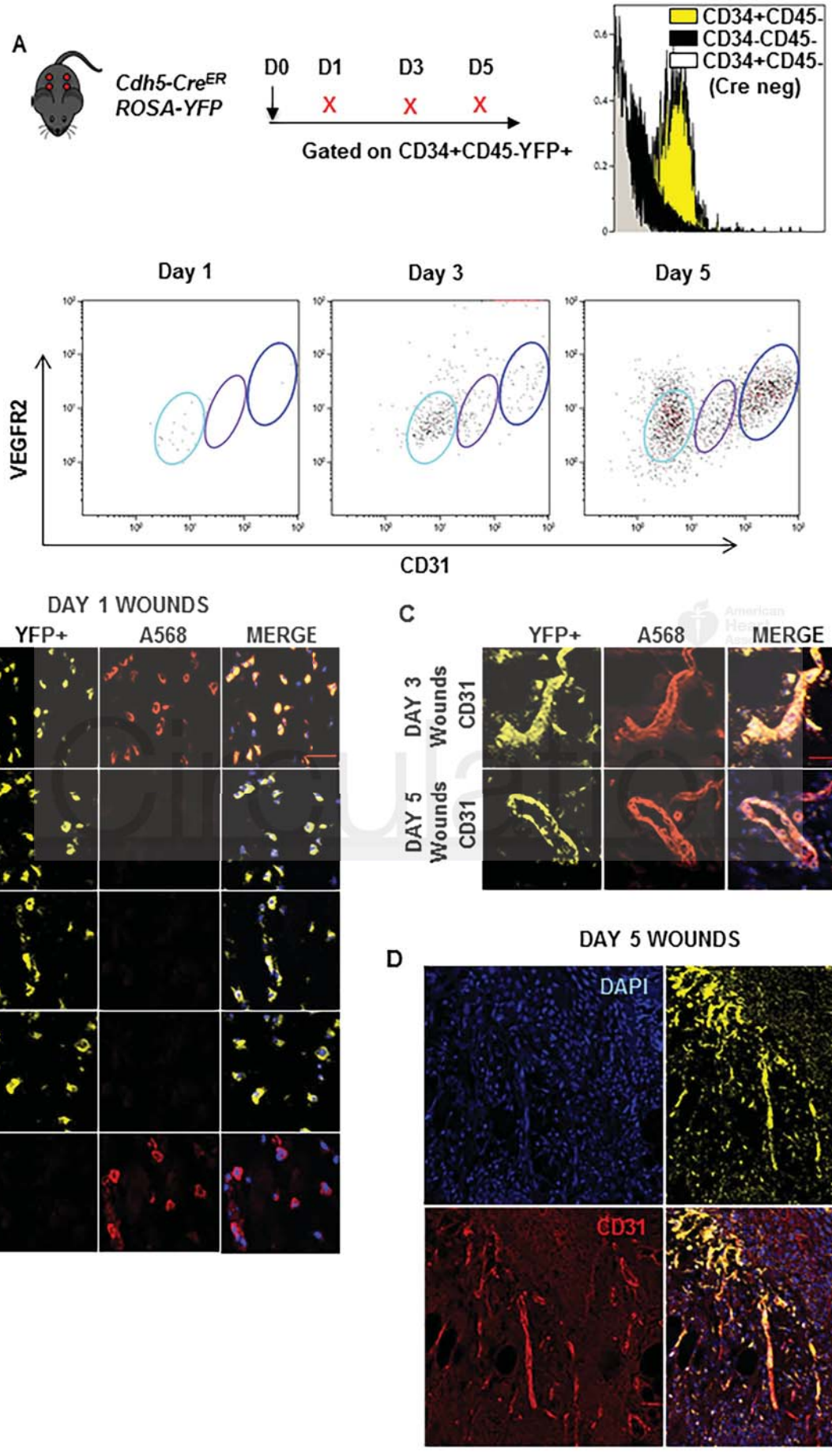

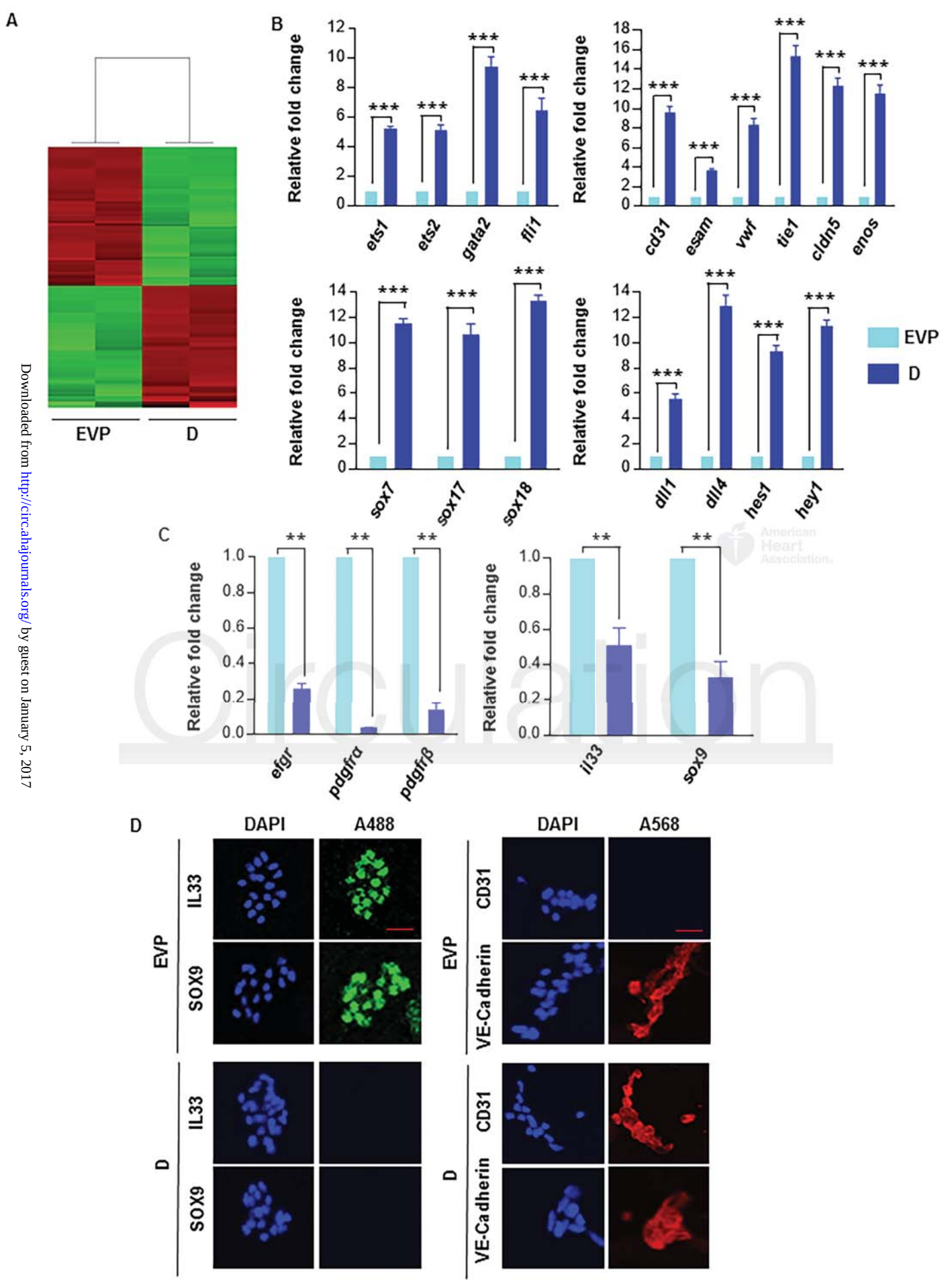

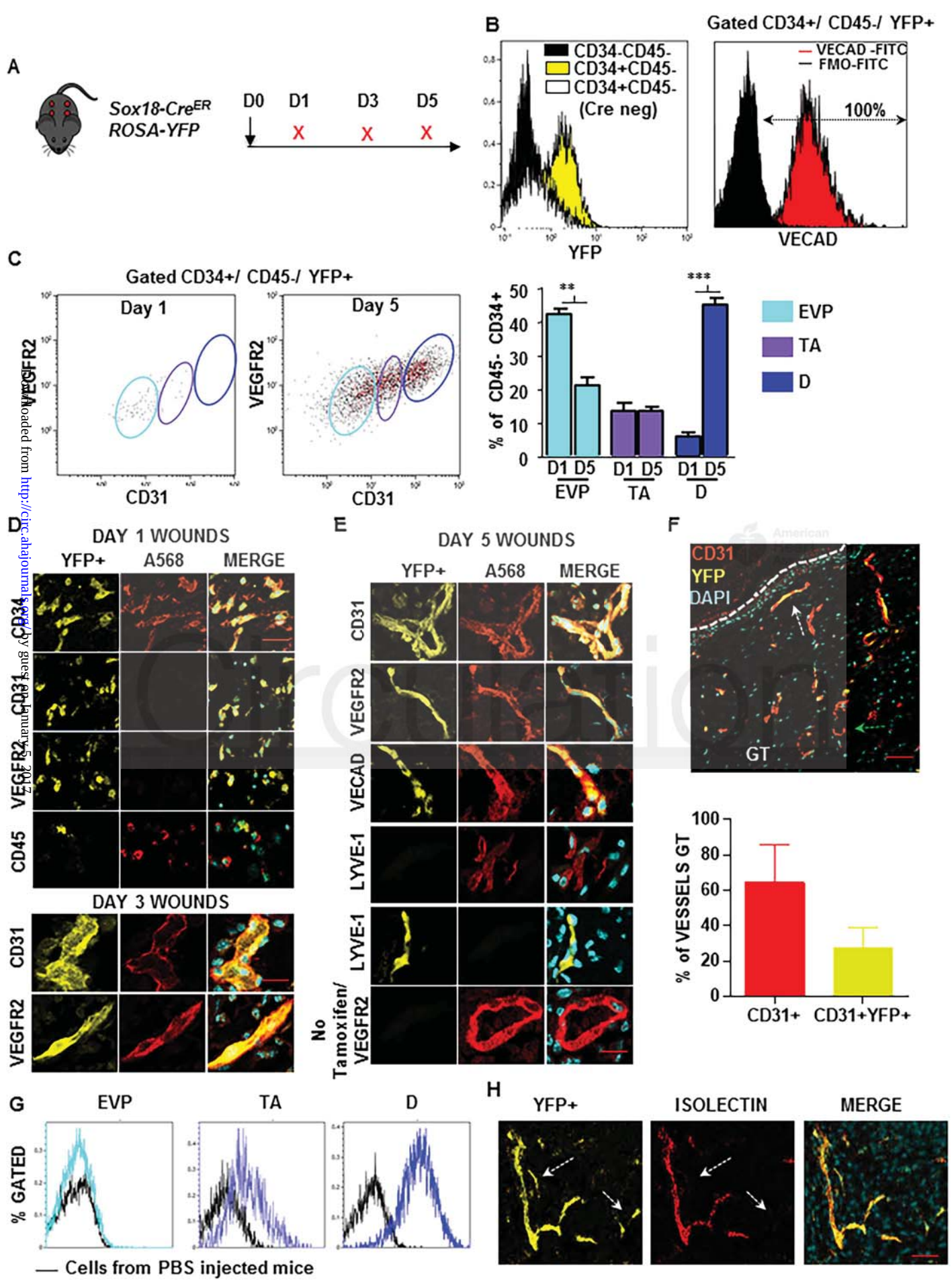

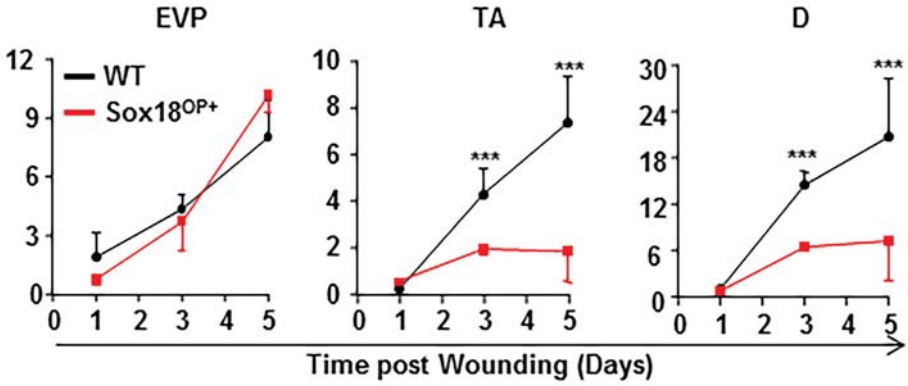

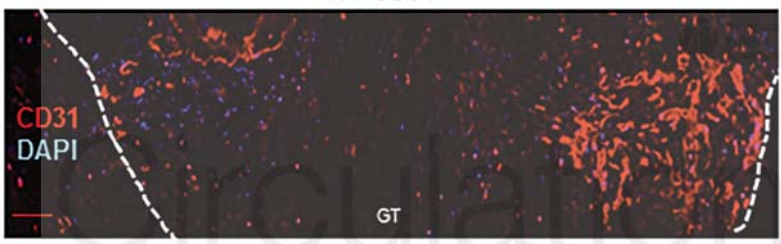

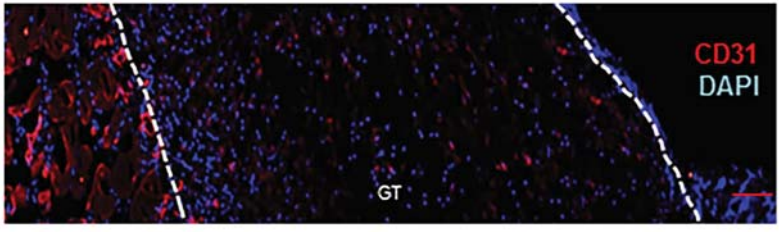

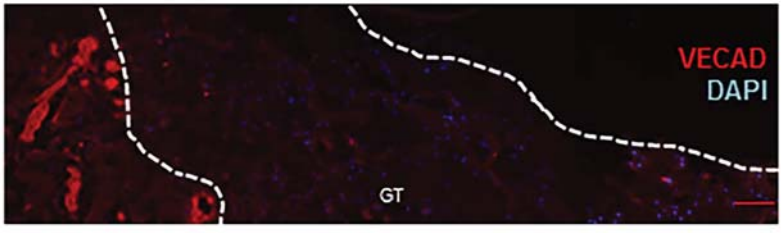

Functional Definition of Progenitors Versus Mature Endothelial Cells Reveals Key SoxF-Dependent Differentiation Process

Jatin Patel, Elke J. Seppanen, Mathieu P. Rodero, Ho Yi Wong, Prudence Donovan, Zoltan Neufeld, Nicholas M. Fisk, Mathias François and Kiarash Khosrotehrani

Circulation. published online November 29, 2016;
Circulation is published by the American Heart Association, 7272 Greenville Avenue, Dallas, TX 75231

Print ISSN: 0009-7322. Online ISSN: 1524-4539

The online version of this article, along with updated information and services, is located on the World Wide Web at:
http://circ.ahajournals.org/content/early/2016/11/29/CIRCULATIONAHA.116.024754

Data Supplement (unedited) at:
http://circ.ahajournals.org/content/suppl/2016/11/29/CIRCULATIONAHA.116.024754.DC1.html

Supplemental Material

Mathematical modeling supports a hierarchy and a differentiation sequence

To understand better the kinetics of endothelial populations in wound granulation tissue, we established mathematical models comparing two scenarios for our data in the context of wound healing using two alternative but complementary methods (Supplementary Figure S1-5). The first was based on EVP giving rise to TA, which then matured to become the D population (Model 1, Supplementary Figure S4A). The second model hypothesized those EVP cells, which appeared first, could give rise to both TA or D cells without any hierarchical distinction (Model 2, Supplementary Figure S4B). Proliferation rates obtained from flow cytometry were applied to each model. We calculated expected proportions of EVP, TA and D according to each model for all possible differentiation variables according to the following equations.

Proliferation rates were considered stable throughout the course of the model and measured values at day 4 (D4) were used to calibrate each population. Finally, apoptosis was estimated to begin from D4 only. Each population could differentiate (therefore reduce its number) towards another population that at each increment of time would consequently increase in addition to its capacity to proliferate.

A-Empiric method

We calculated expected proportions of EVP, TA and D according to each model for all possible differentiation variables according to the following equations:

$$N_P(t) = N_P(t - 1) \times (1+P_{EVP}) - Diff_{EVP\ to\ TA} \times N_P(t - 1) - Diff_{EVP\ to\ D} \times N_P(t - 1)$$

$$N_{TA}(t) = N_{TA}(t - 1) \times (1+P_{TA}) + Diff_{EVP\ to\ TA} \times N_P(t - 1) - Diff_{TA\ to\ D} \times N_{TA}(t - 1) - N_{TA}(t - 1) \times A_{TA}$$

$$N_D(t) = N_D(t - 1) \times (1+P_D) + Diff_{EVP\ to\ D} \times N_P(t - 1) + Diff_{TA\ to\ D} \times N_{TA}(t - 1) - N_D(t - 1) \times A_D$$

where

$N_{EVP}(t)$ = number of EVP cells at time t

$N_{TA}(t)$ = number of TA cells at time t

$N_D(t)$ = number of D cells at time t

These values were obtained from observations for the initial time point at D1 with 158, 193 and 40 for EVP, TA and D respectively.

t = time

P_{EVP} = Proliferation of EVP (calculated from experiments from % of cells in S or G2 phase of the cell cycle)=0.61

P_{TA}= Proliferation of TA (calculated from experiments from % of cells in S or G2 phase of the cell cycle)=0.88

P_D = Proliferation of D (calculated from experiments from % of cells in S or G2 phase of the cell cycle)=0.77

From these parameters the proliferation rates can be obtained as: $r = ln(1+P)$ that gives the following values: r_{EVP} = 0.476, r_{TA} = 0.631, r_D = 0.571

Diff $_{EVP\ to\ TA}$ = differentiation rate from EVP to TA

Diff $_{EVP\ to\ D}$ = differentiation rate from EVP to D

Diff $_{TA\ to\ D}$ = differentiation rate from TA to D

A_{TA} = apoptosis TA =10% from D4

A_D = apoptosis D =10% from D4

We made the following assumptions to simplify the equation

Diff $_{TA\ to\ EVP}$ = 0

Diff $_{D\ to\ EVP}$ = 0

Apoptosis in EVP = 0

and in model 1: Diff $_{EVP\ to\ D}$ = 0.

We then asked whether our expected values differed from our mean observed values by more than 1.96 standard deviations (SDs) by establishing z scores (Supplementary Tables S1-S2). Supplementary Figures S4C-D indicates the number of sub-populations (0-3) that fit the expected values (i.e. average Z score over time was below 1.96). Using the first model, if at each increment in time, 10-60% of EVP cells differentiated into TA and simultaneously 30-70% of TA cells differentiated into definitive D cells, we could obtain kinetics in number (data not shown) and proportion (Supplementary Figure S4F) that matched our observations (Supplementary Figure S4E). However, when we applied differentiation variables in Model 2, we were unable to obtain a single combination where the model fitted within two SDs of our observations for all three sub-populations. Therefore, Model 2 could not substantiate our

observed results (Supplementary Figure S4G) as in any modeled scenario we observed significant divergence from our observations.

B- Best fit method using minimum mean square deviation

To more easily resolve EVP, TA and D cell numbers we adopted a differential equation approach following the same principles and same parameters as defined above.

$$\frac{dN_{EVP}}{dt} = r_{EVP}N_{EVP} - Diff_{EVP\ to\ TA}N_{EVP} - Diff_{EVP\ to\ D}N_{EVP}$$

$$\frac{dN_{TA}}{dt} = r_{TA}N_{TA} + Diff_{EVP\ to\ TA}N_{EVP} - Diff_{TA\ to\ D}N_{TA} - A_{TA}N_{TA}$$

$$\frac{dN_{D}}{dt} = r_{D}N_{D} + Diff_{EVP\ to\ D}N_{EVP} + Diff_{TA\ to\ D}N_{TA} - A_{D}N_{D}$$

The EVP cell population is independent of the other cells and therefore the first equation has a simple exponential solution of the form

$$N_{EVP}(t) = N_{EVP}(0)e^{\alpha t}$$

where $\alpha = r_{EVP} - Diff_{EVP\ to\ TA} - Diff_{EVP\ to\ D}$. We determined the exponent by minimizing the mean square difference from the observations and obtained $\alpha = 0.235$.

Then using the exponential solution for N_{EVP} we can obtain the explicit solutions for the TA and D cells.

In the case of Model 2 the solutions are:

$$N_{TA}(t) = N_{TA}(0)e^{r_{TA}t} + Diff_{EVP\ to\ TA}\frac{N_{EVP}(0)}{r_{TA} - \alpha}(e^{r_{TA}t} - e^{\alpha t})$$

$$N_{D}(t) = N_{D}(0)e^{r_{D}t} + Diff_{EVP\ to\ D}\frac{N_{EVP}(0)}{r_{D} - \alpha}(e^{r_{D}t} - e^{\alpha t})$$

where the unknown parameters are the differentiation rates, with the additional constraint:

$$Diff_{EVP\ to\ TA} + Diff_{EVP\ to\ D} = r_{EVP} - \alpha$$

Comparing with the experimental data, however, we find that the observed growth of the TA cell population is in fact lower than the minimum of the theoretically predicted growth rate corresponding to the case when EVP cells only differentiate into D cells, i.e. $Diff_{EVP\ to\ TA} = 0, Diff_{EVP\ to\ D} = r_{EVP} - \alpha$ with the corresponding solution $N_{TA}(t) = N_{TA}(0)e^{r_{TA}t}$. **In conclusion the observations are not consistent with the predictions of Model 2**.

In the case of Model 1, the predicted growth rate of the TA cell population is reduced by the loss due to their differentiation into D cells. In this case the solutions for the cell numbers are:

$$N_{TA}(t) = N_{TA}(0)e^{(r_{TA} - Diff_{TA\ to\ D})t} + Diff_{EVP\ to\ TA}\frac{N_{EVP}(0)}{r_{TA} - Diff_{TA\ to\ D} - \alpha}(e^{(r_{TA} - Diff_{TA\ to\ D})t} - e^{\alpha t})$$

where $Diff_{EVP\ to\ TA} = r_{EVP} - \alpha$ = 0.241, and

$$N_D(t) = \left[N_D(0) + \frac{Diff_{TA\ to\ D}}{r_D - r_{TA} + Diff_{TA\ to\ D}}\left(N_{TA}(0) + \frac{Diff_{EVP\ to\ TA}N_{EVP}(0)}{r_{TA} - Diff_{TA\ to\ D} - \alpha}\right) - \frac{Diff_{TA\ to\ D}Diff_{EVP\ to\ TA}N_{EVP}(0)}{(r_{TA} - Diff_{TA\ to\ D} - \alpha)(r_D - \alpha)}\right]e^{r_D t} - \frac{Diff_{TA\ to\ D}}{r_D - r_{TA} + Diff_{TA\ to\ D}}\left(N_{TA}(0) + \frac{Diff_{EVP\ to\ TA}N_{EVP}(0)}{r_{TA} - Diff_{TA\ to\ D} - \alpha}\right)e^{(r_{TA} - Diff_{TA\ to\ D})t} + \frac{Diff_{EVP\ to\ TA}N_{EVP}(0)}{(r_{TA} - Diff_{TA\ to\ D} - \alpha)(r_D - \alpha)}e^{\alpha t}$$

Note, that in both solutions the only unknown parameter is $Diff_{EVP\ to\ TA}$. We found that the mean square deviation from the experimental data is minimized for: $Diff_{TA\ to\ D} = 0.26$.

So overall, differentiation rates from EVP to TA and from TA to D have a best fit at 0.241 and 0.26 respectively which is consistent with the intervals suggested by the empirical method, Of note both methods do not find any solution for model 2 where EVP gives rise to both TA and D.

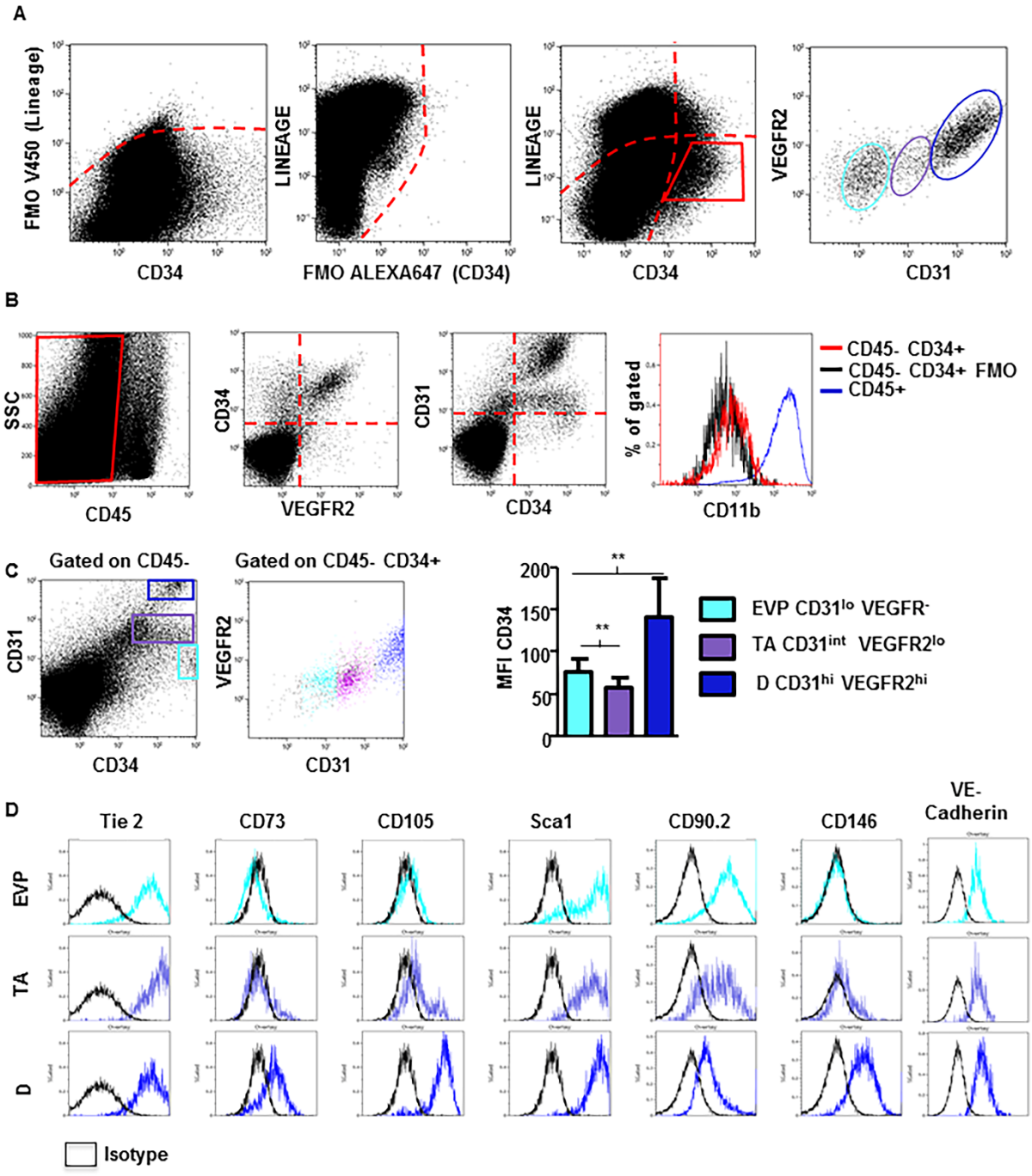
A
FMO V450 (Lineage)
CD34
LINEAGE
FMO ALEXA647 (CD34)
LINEAGE
CD34
VEGFR2
CD31
B
SSC
CD45
CD34
VEGFR2
CD31
CD34
% of gated
CD11b
CD45- CD34+
CD45- CD34+ FMO
CD45+
C
Gated on CD45-
Gated on CD45- CD34+
CD31
CD34
VEGFR2
CD31
MFI CD34
200
150
100
50
0
**
**
EVP CD31lo VEGFR-
TA CD31int VEGFR2lo
D CD31hi VEGFR2hi
D
Tie 2
CD73
CD105
Sca1
CD90.2
CD146
VE-Cadherin
EVP
TA
D
Isotype

E

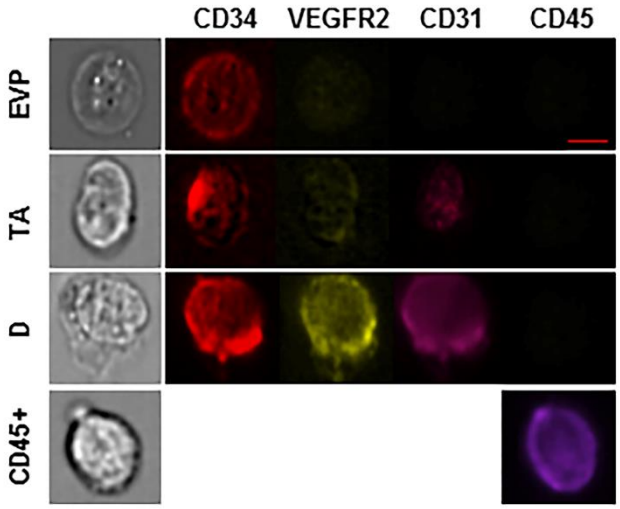
CD34
VEGFR2
CD31
CD45
EVP
TA
D
CD45+

F

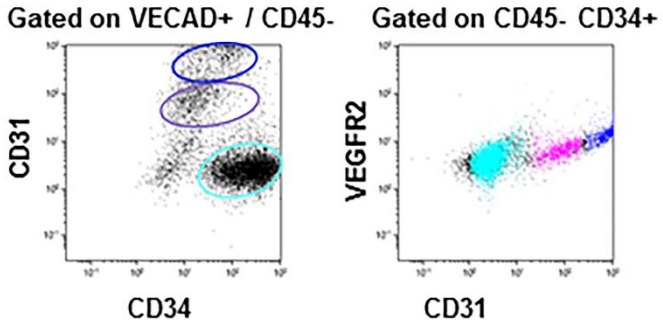
Gated on VECAD+ / CD45-
Gated on CD45- CD34+
CD31
CD34
VEGFR2
CD31

Supplementary Figure S1: Characterization of endothelial heterogeneity using flow cytometry. A, Flow plots (restricted to live gate) represent the exclusion of Lineage+ cells and subsequent gating on Lineage-CD34+ cells displays the presence of three populations based on CD31 and VEGFR2 levels: from left to right: EVP, TA and D. **B,** shows that among CD45- cells, all CD31+ or VEGFR2+ cells express some level of CD34 based on FMO (threshold figured in dashed lines) (n=6). All CD34+CD45- cells were also CD11b-, a marker of monocyte/macrophage populations. **C,** Gated CD45- cells can be discriminated based on CD34 and CD31 levels of expression. In the upper right quadrant representing the endothelial cells, three populations of cells can be distinguished (CD34hi CD31lo (blue), CD34lo and CD31int (purple) and finally CD31hiCD34hi (dark blue). These populations correspond to the described EVP, TA and D as defined by their levels of CD31 and VEGFR2. The level of CD34 was quantified based on Mean-Fluorescence-Intensity (MFI) for each of the endothelial populations. Results presented as mean +/- SEM (**p<0.01; n=3). **D,** Histogram plots further characterizing the three endothelial populations for a range of cell surface markers from cells obtained at day 5 post wounding. **E,** Amnis® analysis combining flow cytometry and imaging of single cells confirmed cell surface marker expression levels (Scale bar represents 30µm; representative images of n=3).**F,** Using aorta obtained from uninjured mice we demonstrate the existence of the 3 endothelial populations based on CD31, CD34 and VEGFR2 levels (n=4). Results presented as mean +/- SEM. EVP – Endovascular Progenitor; TA – Transit Amplifying; D – Definitive Differentiated

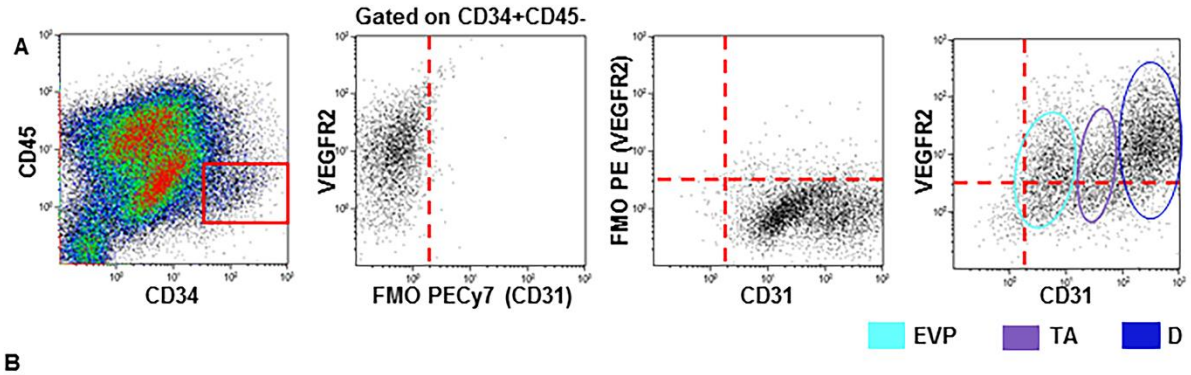
A
Gated on CD34+CD45-
CD45
CD34
VEGFR2
FMO PECy7 (CD31)
FMO PE (VEGFR2)
CD31
VEGFR2
CD31
EVP
TA
D

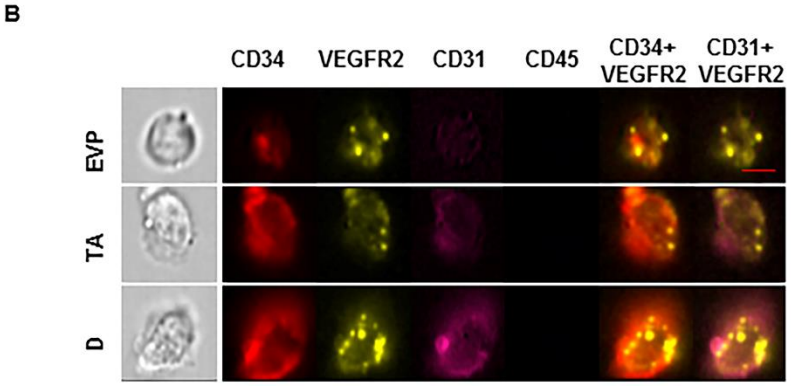
B
CD34
VEGFR2
CD31
CD45
CD34+ VEGFR2
CD31+ VEGFR2
EVP
TA
D

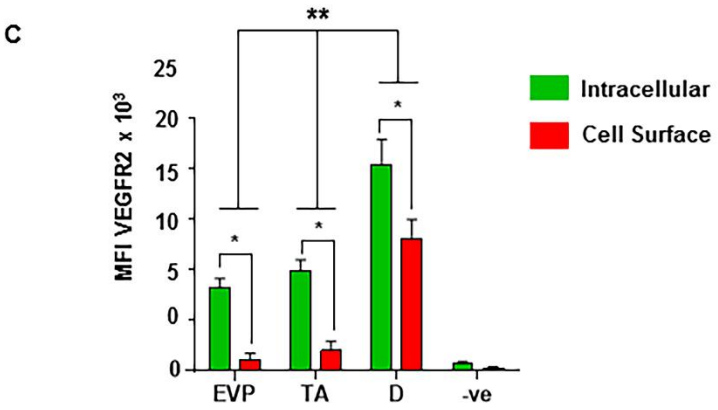
C
**
*
*
*
MFI VEGFR2 x 10³
25
20
15
10
5
0
0
EVP
TA
D
-ve
Intracellular
Cell Surface

Supplementary Figure S2: Intracellular expression of CD31 and VEGFR2. A, Fluorescence-Minus-One (FMO) analyses were performed on cells from D5 wounds in order to set threshold for CD31 and VEGFR2 intracellular protein staining, on all surface CD34+CD45- gated cells. CD31 intracellular staining was similar to cell surface staining (CD31lo, CD31int, CD31hi), whereas all populations expressed intracellular VEGFR2 at a higher level. **B,** Amnis® analysis combining flow cytometry and imaging of single cells confirmed the intracellular marker expression for VEGFR2 but not CD31 (Scale bar represents 30µm; representative images of n=3). **C,** Quantification of cell surface versus intracellular VEGFR2 staining using Amnis® images further confirmed the increase in VEGFR2 intracellular expression between the three endothelial populations (*$p<0.05$ Intracellular vs cell surface; **$p<0.01$ D vs EVP or TA; n=3). Results presented as mean +/- SEM.

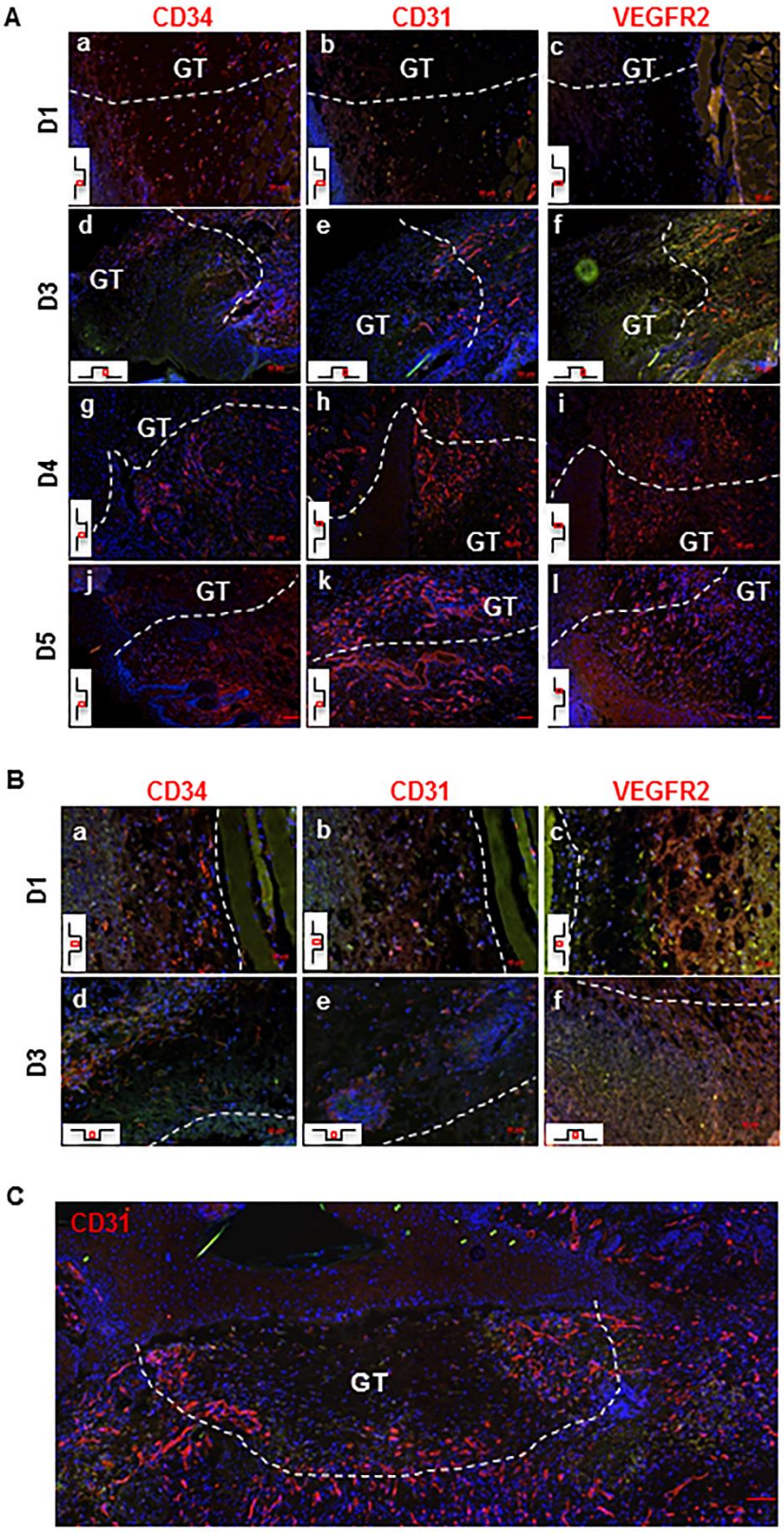
A
CD34
CD31
VEGFR2
D1
D3
D4
D5
a
b
c
d
e
f
g
h
i
j
k
l
GT
B
CD34
CD31
VEGFR2
D1
D3
a
b
c
d
e
f
C
CD31
GT

Supplementary Figure S3. Evolution of vascular marker staining on wound sections over time. Wound edge: **A,** IHC staining with CD34 **(a, d, g, j)**, CD31 **(b, e, h, k)** and VEGFR2 **(c, f, i, l)** confirm the sequential appearance of the endothelial markers. Blood vessels labeled with all three markers infiltrate the granulation tissue (GT) from the wound edge (represented by the white dotted line). This can be clearly seen in D3 wounds **(d-f)** (n=3). Wound center: **B,** IHC staining with CD34 **(a-d)**, CD31 **(b-e)** and VEGFR2 **(c-f)** confirm the absence of blood vessels in GT (n=3). Inserts in the bottom left corner depict the orientation of the wound. The red box indicates the approximate region where the image was taken. **C,** Representative D4 wound section stained with CD31. White dotted line represents wound edge (Scale bars in whole figure represents 150μm; n=3).

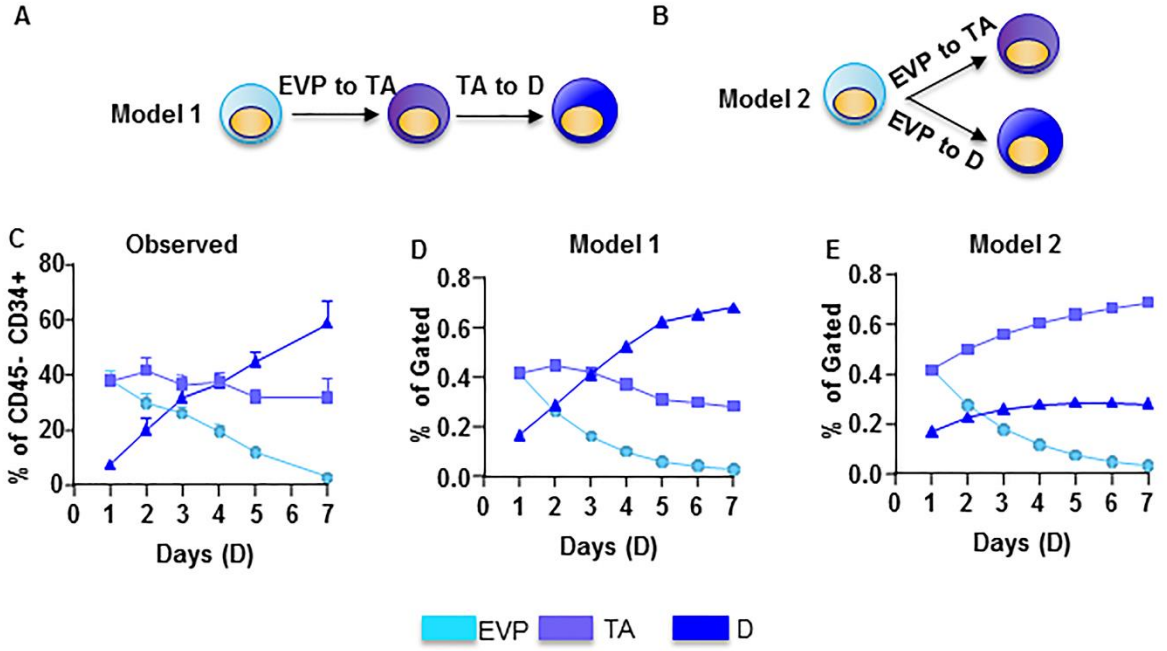

F

EVP → TA differentiation

TA → D differentiation

%	10	20	30	40	50	60	70	80	90
10	2	2	2	1	2	2	1	1	1
20	3	2	2	2	2	2	1	1	1
30	3	3	3	2	2	2	1	1	1
40	3	3*	3	3	3	3	1	1	1
50	3	3*	3*	3	3	3	2	2	2
60	3	3	3	3	3	3	2	2	2
70	2	3	3	3	3	3	1	1	1
80	2	2	1	2	2	2	1	1	1
90	2	2	1	1	1	2	1	1	1

G

EVP → D differentiation

%	10	20	30	40	50	60	70	80	90
10	1	1	1	1	1	1	0	0	0
20	2	2	1	1	1	0	0	0	
30	2	2	2	2	1	1	1		
40	2	2	2	1	1	1			
50	2	2	1	1	1				
60	2	1	1	1					
70	1	1	1						
80	1	1							
90	1								

ns <1.96 SD <1 SD

Supplementary Figure S4. Mathematical modeling of murine endothelial hierarchy. Two hypothetical models were devised (Model 1 and 2) to investigate the plausibility of hierarchical differentiation. **A**-Model 1 was based on EVP giving rise to TA, which then matured to become the D population whereas **B**-Model 2 hypothesized that EVP cells could give rise to both TA or D cells without any hierarchical distinction. **C-D,** Displayed is a representation of sub-populations that fit expected values. For example: 3 means that all three populations had observations within 2 standard deviation of the values calculated according to the model. Bold values in green represent those differentiation rates when all three sub-populations (0-3) were within 1.96 SDs of the observed values. In blue were figured the situations where all populations were within 1 SD of the mean from the calculated values. Finally * indicates situations where differences were below 1SD at every single time point for all three populations highlighting the quality of the model to reproduce our observations. This type of analysis supported the differentiation of the endothelial hierarchy presented in Model 1 and that of our observed data (n=6) over (**E)** Model 2. **F-G** Model 2 could not substantiate our observed values when we applied differential variables. EVP – Endovascular Progenitor; TA – Transit Amplifying; D – Definitive Differentiated.

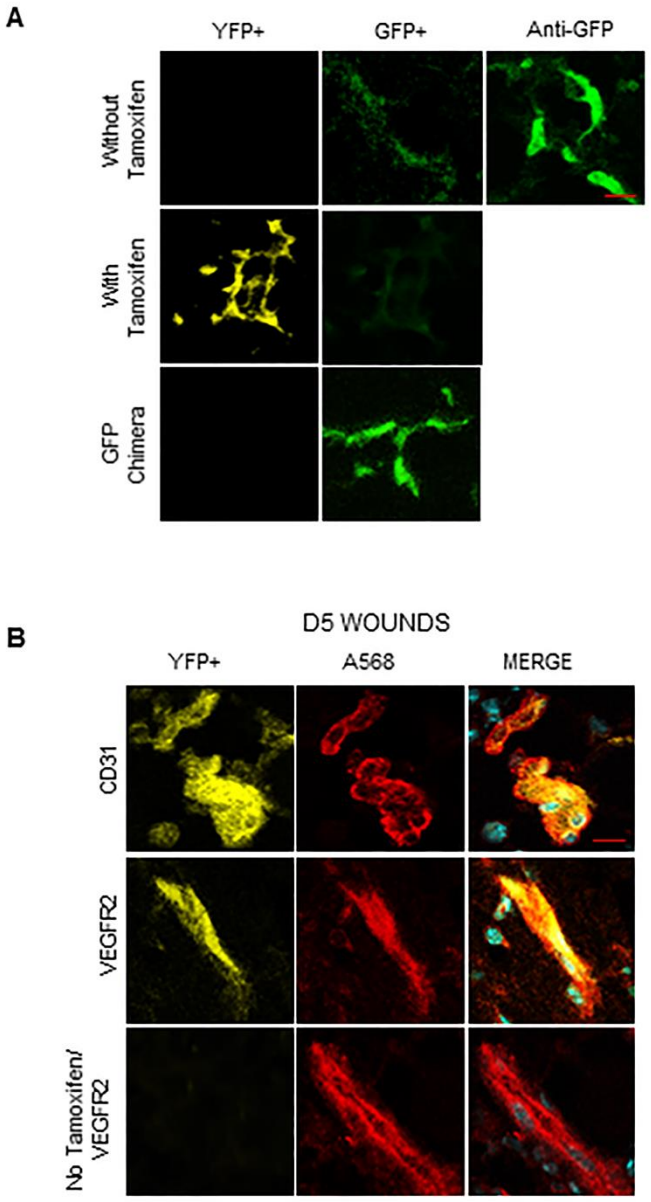
A
YFP+
GFP+
Anti-GFP
Without Tamoxifen
With Tamoxifen
GFP Chimera
B
D5 WOUNDS
YFP+
A568
MERGE
CD31
VEGFR2
No Tamoxifen/ VEGFR2

Figure S5. Lineage tracing using *Sox18-cre^{ERt2}/Rosa-YFP* mice. A, Representative images demonstrating our capacity to differ between GFP and YFP signals using confocal microscopy. The *Sox18-cre^{ERt2}* also expresses *GFP* under the control of the *Sox18* promoter. Without tamoxifen, only the GFP signal in *Sox18-cre^{ERt2}/Rosa-YFP* could be detected especially upon use of anti-GFP antibodies. Once tamoxifen was administered, the YFP signal could be detected and separated from the GFP (Scale bar represents 50μm; n=2). Finally, GFP signal obtained from chimeric mice with a GFP transgenic bone marrow was not detected using our settings to obtain YFP signal. **B,** Lineage tracing using *Sox18-cre^{ERt2}/Rosa-YFP* mice, injected on a daily basis from D0 to D5 labelled all blood vessels. Immunofluorescence images demonstrating CD31 and VEGFR2 staining on YFP+ vessels at D5 post-wounding (Scale bar represents 50μm; n=6). EVP – Endovascular Progenitor; TA – Transit Amplifying; D – Definitive Differentiated. YFP – Yellow Fluorescent Protein; GFP – Green Fluorescent Protein; A568 – Alexa 568 secondary stain (Red).

Supplementary Table S1: Z scores comparing Model 1 tour observed value

P → TA differentiation

TA → D differentiation

a

P	10	20	30	40	50	60	70	80	90
10	0.75	0.30	0.61	1.05	1.42	1.73	1.99	2.21	2.40
20	**0.77**	0.31	0.60	1.04	1.42	1.73	1.99	2.21	2.40
30	**0.79**	**0.32**	**0.59**	1.03	1.41	1.72	1.99	2.21	2.39
40	**0.80**	**0.33**	**0.58**	**1.03**	**1.40**	**1.72**	1.99	2.21	2.39
50	**0.82**	**0.34**	**0.57**	**1.02**	**1.40**	**1.72**	1.98	2.21	2.39
60	**0.83**	**0.35**	**0.56**	**1.01**	**1.39**	**1.71**	1.98	2.20	2.39
70	0.85	**0.36**	**0.55**	**1.01**	**1.39**	**1.71**	1.98	2.20	2.39
80	0.86	0.37	0.54	1.00	1.38	1.71	1.98	2.20	2.39
90	0.87	0.37	0.54	0.99	1.38	1.70	1.97	2.20	2.39

b

TA	10	20	30	40	50	60	70	80	90
10	2.54	3.12	3.63	4.07	4.45	4.78	5.06	5.30	5.50
20	**1.55**	2.11	2.59	3.01	3.36	3.67	3.93	4.16	4.34
30	**0.66**	**1.19**	**1.65**	2.04	2.38	2.66	2.91	3.11	3.28
40	**0.75**	**0.72**	**0.82**	**1.17**	**1.48**	**1.75**	1.98	2.16	2.32
50	**1.18**	**0.82**	**0.82**	**0.91**	**1.02**	**1.18**	1.35	1.51	1.66
60	**1.82**	**1.36**	**0.97**	**0.94**	**1.03**	**1.15**	1.28	1.41	1.54
70	2.38	**1.95**	**1.59**	**1.28**	**1.04**	**1.13**	1.26	1.39	1.51
80	2.88	2.47	2.13	1.84	1.60	1.40	1.26	1.33	1.45
90	3.32	2.94	2.61	2.34	2.12	1.94	1.79	1.68	1.66

c

D	10	20	30	40	50	60	70	80	90
10	2.01	2.00	1.98	1.97	1.96	1.95	1.94	1.93	1.92
20	**1.30**	1.26	1.23	1.20	1.17	1.14	1.12	1.09	1.07
30	**0.67**	**0.61**	**0.55**	0.50	0.45	0.41	0.37	0.34	0.30
40	**0.18**	**0.21**	**0.27**	**0.32**	**0.37**	**0.41**	0.45	0.48	0.52
50	**0.52**	**0.62**	**0.71**	**0.80**	**0.88**	**0.95**	1.02	1.08	1.13
60	**0.96**	**1.08**	**1.19**	**1.30**	**1.39**	**1.48**	1.56	1.63	1.69
70	1.35	**1.49**	**1.62**	**1.74**	**1.85**	**1.95**	2.04	2.12	2.19
80	1.69	1.85	2.00	2.13	2.25	2.36	2.46	2.56	2.64
90	1.98	2.16	2.32	2.47	2.61	2.73	2.84	2.94	3.04

Supplementary Table S2: Z scores comparing Model 2 to our observed values

P → TA differentiation

P ↑ D differentiation

a

P	10	20	30	40	50	60	70	80	90
10	0.52	0.36	0.85	1.26	1.61	1.90	2.15	2.35	2.52
20	0.35	0.84	1.26	1.61	1.90	2.14	2.35	2.52	
30	0.83	1.25	1.61	1.90	2.14	2.35	2.51		
40	1.25	1.60	1.90	2.14	2.34	2.51			
50	1.60	1.89	2.14	2.34	2.51				
60	1.89	2.14	2.34	2.51					
70	2.14	2.34	2.51						
80	2.34	2.51							
90	2.51								

b

TA	10	20	30	40	50	60	70	80	90
10	3.27	3.90	4.45	4.93	5.35	5.71	6.02	6.29	6.52
20	3.21	3.81	4.33	4.78	5.18	5.53	5.82	6.08	
30	3.16	3.72	4.22	4.65	5.02	5.35	5.63		
40	3.11	3.64	4.11	4.52	4.88	5.19			
50	3.07	3.57	4.01	4.40	4.74				
60	3.02	3.50	3.92	4.28					
70	2.98	3.43	3.83						
80	2.94	3.37							
90	2.91								

c

D	10	20	30	40	50	60	70	80	90
10	2.34	2.38	2.41	2.45	2.48	2.51	2.53	2.56	2.58
20	1.89	1.96	2.02	2.08	2.13	2.18	2.23	2.27	
30	1.50	1.59	1.68	1.75	1.83	1.89	1.95		
40	1.16	1.27	1.38	1.47	1.56	1.64			
50	0.87	1.00	1.12	1.23	1.33				
60	0.72	0.86	0.99	1.11					
70	0.60	0.75	0.89						
80	0.58	0.69							
90	0.62								

Supplementary Table S3: Primer list for qPCR

Gene	Forward Primer	Reverse Primer
β-actin	GTGACGTTGACATCCGTAAAGA	GCCGGACTCATCGTACTCC
Cd34	CGAGTGCCATTAAGGGAGAAA	CACTTAGTTCCAGGCAGATACC
Cd45	GAGTGCAAAGGAGACCCTATTT	TGTGTCCAGAAGGGCAAATC
Cd31	GCCAAGGCCAAACAGAAAC	CTTCCACACTAGGCTCAGAAAT
Vegfr2	GTGTACATCACCGAGAACAAGA	CTGGATACCTAGCGCAAAGAG
Tie1	GCCCTCGGATTTGGTAGGC	CCGTGTGTGTGACCTTGTCT
Vwf	CTCTTTGGGGACGACTTCATC	TCCCGAGAATGGAGAAGGAAC
Cdh5	CCACTGCTTTGGGAGCCTT	GGCAGGTAGCATGTTGGGG
Egfr	ATGAAAACACCTATGCCTTAGCC	TAAGTTCCGCATGGGCAGTTC
Pdgfrα	ATGAGAGTGAGATCGAAGGCA	CGGCAAGGTATGATGGCAGAG
Pdgfrβ	CATCCGCTCCTTTGATGATCTT	GTGCTCGGGTCATGTTCAAGT
Gata2	AAGGATGGCGTCAAGTACCAA	TATCGGGTGGTGTGTTGCAG
Fli1	TTGATTCAGCATACGGAGCGG	CACTGGCTGGTTGATCCACTC
Enos	TCAGCCATCACAGTGTTCCC	ATAGCCCGCATAGCGTATCAG
Esam	TTGCTGCGGGTTTTGTTCCT	TCTACCGCTTCCAATTTGTTGAG
Cldn5	GCAAGGTGTATGAATCTGTGCT	GTCAAGGTAACAAAGAGTGCCA
Ets1	TCCTATCAGCTCGGAAGAACTC	TCTTGCTTGATGGCAAAGTAGTC
Ets2	CCTGTCGCCAACAGTTTTCG	GGAGTGTCTGATCTTCACTGAGA
Dll1	CCCATCCGATTCCCCTTCG	GGTTTTCTGTTGCGAGGTCATC
Dll4	TTCCAGGCAACCTTCTCCGA	ACTGCCGCTATTCTTGTCCC
Hes1	TCAGCGAGTGCATGAACGAG	CATGGCGTTGATCTGGGTCA
Hey1	CCGACGAGACCGAATCAATAAC	TCAGGTGATCCACAGTCATCTG
Il33	ATTTCCCCGGCAAAGTTCAG	AACGGAGTCTCATGCAGTAGA
Sox7	TGGACACGTATCCCTACGGG	TCCTGACATGAGGACGAGAAG
Sox17	CCAAAGCGGAGTCTCGCAT	GCCTAGCATCTTGCTTAGCTC
Sox18	CCTGTCACCAACGTCTCGC	CAAAGCCATAGCGCCCTGA
Sox9	AGTACCCGCATCTGCACAAC	ACGAAGGGTCTCTTCTCGCT